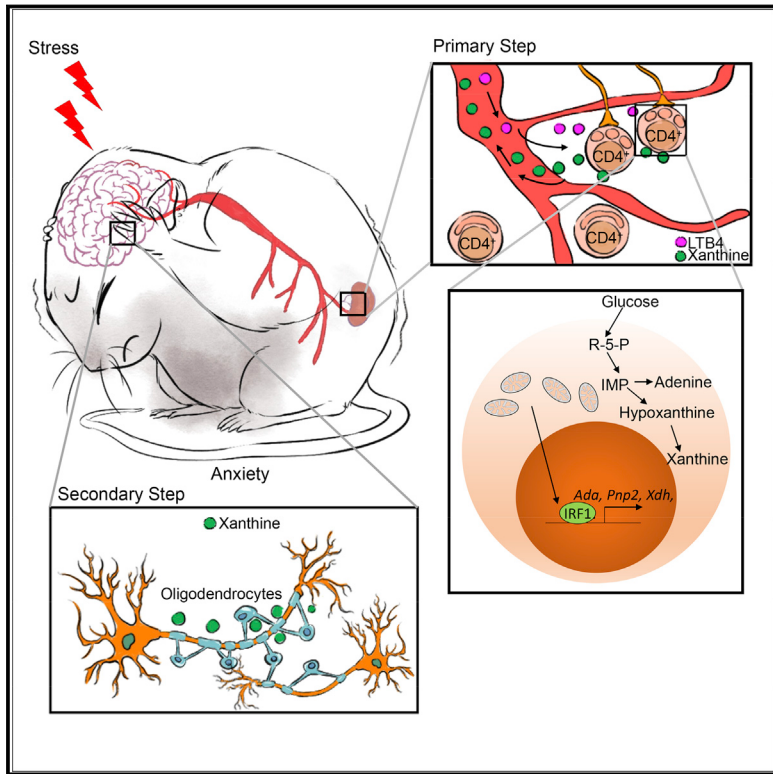


Stress-Induced Metabolic Disorder in Peripheral CD4⁺ T Cells Leads to Anxiety-like Behavior

Graphical Abstract



Authors

Ke-qi Fan, Yi-yuan Li, Hao-li Wang, ...,
Xin-Hua Feng, Ren-jie Chai, Jin Jin

Correspondence

jjin4@zju.edu.cn (J.J.),
renjiec@seu.edu.cn (R.-j.C.)

In Brief

Xanthine metabolism in CD4⁺ T cells is found to be central to mediating the effects of stress-induced anxiety like behavior in mice through its effects on oligodendrocyte proliferation and neuronal hyperactivation.

Highlights

- Peripheral CD4⁺ T cells control stress-induced anxiety-like behavior
- Mitochondrial fission in peripheral CD4⁺ T cell causes severe anxiety symptoms
- T cell-derived xanthine acts on the oligodendrocytes in the left amygdala
- IRF-1 controls purine synthesis in CD4⁺ T cells and triggers the onset of anxiety



Stress-Induced Metabolic Disorder in Peripheral CD4⁺ T Cells Leads to Anxiety-like Behavior

Ke-qi Fan,^{1,9} Yi-yuan Li,^{1,9} Hao-li Wang,¹ Xin-tao Mao,¹ Jin-xin Guo,¹ Fei Wang,¹ Ling-jie Huang,² Yi-ning Li,¹ Xiang-yu Ma,^{3,4,5} Zheng-jun Gao,¹ Wei Chen,⁶ Dan-dan Qian,³ Wen-jin Xue,³ Qian Cao,² Lei Zhang,² Li Shen,¹ Long Zhang,¹ Chao Tong,¹ Jiang-yan Zhong,¹ Wei Lu,³ Ling Lu,⁷ Ke-ming Ren,² Guisheng Zhong,⁸ Yuan Wang,⁶ Mingliang Tang,³ Xin-Hua Feng,¹ Ren-jie Chai,^{3,4,5,*} and Jin Jin^{1,2,10,*}

¹MOE Laboratory of Biosystem Homeostasis and Protection and Life Sciences Institute, Zhejiang University, Hangzhou 310058, China

²Sir Run Run Shaw Hospital, College of Medicine, Zhejiang University, Hangzhou 310016, China

³Key Laboratory for Developmental Genes and Human Disease, Ministry of Education, Institute of Life Sciences, Jiangsu Province High-Tech Key Laboratory for Bio-Medical Research, Southeast University, Nanjing 210096, China

⁴Co-Innovation Center of Neuroregeneration, Nantong University, Nantong 226001, China

⁵Institute for Stem Cell and Regeneration, Chinese Academy of Science, Beijing, China

⁶Shanghai Key Laboratory of Regulatory Biology, Institute of Biomedical Sciences and School of Life Sciences, East China Normal University, 500 Dongchuan Road, Shanghai 200241, China

⁷Department of Otolaryngology Head and Neck Surgery, Nanjing Drum Tower Hospital, Nanjing University Medical School, Nanjing, 210008, Jiangsu, China

⁸iHuman Institute, ShanghaiTech University, Shanghai 201210, China

⁹These authors contributed equally

¹⁰Lead contact

*Correspondence: jjin4@zju.edu.cn (J.J.), renjiec@seu.edu.cn (R.-j.C.)

<https://doi.org/10.1016/j.cell.2019.10.001>

SUMMARY

Physical or mental stress leads to neuroplasticity in the brain and increases the risk of depression and anxiety. Stress exposure causes the dysfunction of peripheral T lymphocytes. However, the pathological role and underlying regulatory mechanism of peripheral T lymphocytes in mood disorders have not been well established. Here, we show that the lack of CD4⁺ T cells protects mice from stress-induced anxiety-like behavior. Physical stress-induced leukotriene B4 triggers severe mitochondrial fission in CD4⁺ T cells, which further leads to a variety of behavioral abnormalities including anxiety, depression, and social disorders. Metabolomic profiles and single-cell transcriptome reveal that CD4⁺ T cell-derived xanthine acts on oligodendrocytes in the left amygdala via adenosine receptor A1. Mitochondrial fission promotes the *de novo* synthesis of purine via interferon regulatory factor 1 accumulation in CD4⁺ T cells. Our study implicates a critical link between a purine metabolic disorder in CD4⁺ T cells and stress-driven anxiety-like behavior.

INTRODUCTION

Emotional reactions, including fear and stress, are considered normal psychological and physical reactions to positive or negative situations in our lives. However, frequent acute emotional reactions referred to as chronic stress (CS) are pathological conditions that increase the risk of depression and anxiety (de Kloet

et al., 2005; Krishnan and Nestler, 2008; McEwen et al., 2015).

Most of the current therapeutic drugs for anxiety or depression, such as selective monoamine neurotransmitter re-uptake inhibitors, directly target the central nervous system (CNS). However, these drugs are accompanied by many side effects, including sexual dysfunction, systemic metabolic disorder, and persistent hypertension. Therefore, it is of great significance to understand the pathogenesis of mood disorders to develop nontraditional therapeutic drugs.

In addition to causing anxiety behaviors, stress can lead to disorders of the immune, metabolic, and cardiovascular systems (Dimsdale, 2008; Glaser and Kiecolt-Glaser, 2005; Reiche et al., 2004; Tamashiro et al., 2011). Acute-stress conditions appear to enhance the immune response, while CS diminishes immune responses, including decreasing leukocyte trafficking, impairing neutrophil phagocytosis, and reducing the number of peripheral lymphocytes (Glaser and Kiecolt-Glaser, 2005; Padgett and Glaser, 2003). Some recent studies have also highlighted the physiological function of various immune molecules in the onset of anxiety-like behaviors. IL-6 and IL-1 β derived from innate immune cells can affect many aspects of the CNS, including neurotransmitter metabolism, neuronal endocrine function, and neuroplasticity in a mouse model (Chourbaji et al., 2006; Engler et al., 2017; McKim et al., 2018; Wakabayashi et al., 2015). Adaptive immunity is also involved in the maintenance of the CNS and is relevant to stress-triggered behaviors, including anxiety (Filiano et al., 2016). IFN- γ derived from meningeal T cells acts on neurons in the prefrontal cortex (PFC) to promote GABAergic inhibition and prevent abnormal excitability (Filiano et al., 2016). Programmed Cell Death 1 KO (*Pdcd1*^{-/-}) T cells exhaust tryptophan (Trp) and tyrosine, which leads to substantial deficiencies in neurotransmitters and anxiety-like behavior



(Miyajima et al., 2017). However, multiple questions regarding the effect of T cells on the onset of anxiety remain to be answered, including (1) the physiological functions of T lymphocytes in stress-induced anxiety-like behavior, (2) whether stress-induced anxiety is dependent on the activation of peripheral T cells or not, (3) the imprinting characteristics of pathological T cells in mood disorders, and (4) the molecular mechanism by which pathological T cells regulate the activity of neuronal or nonneuronal cells in the CNS.

RESULTS

CD4⁺ T Cells Are Essential Components of Stress-Induced Anxiety Behaviors

To examine the role of the adaptive immune system in stress-induced behavioral changes, we exposed wild-type (WT) or recombination activating gene 1 (*Rag1*)^{-/-} mice to electronic foot shock (ES) for 8 consecutive days to induce an anxiety model (Bourin et al., 2007; Campos et al., 2013; Steimer, 2011) (Figure 1A). In contrast to WT mice, immunodeficient *Rag1*^{-/-} mice did not exhibit reduced interest in exploring the central region and locomotion in the open-field test (OFT) (Figure 1B), implying that the adaptive immunity is required for the onset of anxiety. Consistent with previous reports (Dhabhar, 2008; Dragos and Tanasescu, 2010), mice with acute ES exposure exhibited significantly increased frequencies and numbers of peripheral CD4⁺ and CD8⁺ lymphocytes compared to those of nontreated (NT) controls (Figures S1A and S1B).

To investigate which subpopulation of lymphocytes is involved in ES-induced mood disorders, we depleted CD4⁺ or CD8⁺ T cells by intravenous (i.v.) injection with neutralizing antibodies before inducing the ES model (Figure 1A) and verified the removal efficiencies by fluorescence-activated cell sorting (FACS) analysis (Figure S1C). Surprisingly, only CD4⁺ T cell depletion significantly reversed the ES-induced anxiety-like behavior in the OFT and elevated plus-maze (EPM) test (Figures 1C and 1D). To further confirm the role of CD4⁺ T cells in CS, we extended the procedures of the ES models to 30 days. As shown in Figure S1D, CD4⁺ T cells were also required for chronic ES-induced anxiety-like behavior. In contrast to the ES model, an acute restraint stress (RS) model reduced the frequency of CD4⁺ T cells (Figure S1E), which is consistent with observations in patients with anxiety (Figure S1F). However, CD4⁺ T cell deficiency still prevented RS-treated mice from developing anxiety (Figure 1E), suggesting that CD4⁺ T cells have a broad impact on physical stress-induced anxiety-like behavior.

To assess whether T cells retain anxiety imprints, NT or ES-induced splenic CD4⁺ or CD8⁺ T cells were adoptively transferred into *Rag1*^{-/-} mice (Figure 1F). Only the *Rag1*^{-/-} mice that received ES-induced CD4⁺ T cells developed anxiety-like behavior in the OFT (Figure 1G). Surprisingly, the NT CD4⁺ T cells induced weak anxiety-like symptoms, suggesting that some natural products derived from CD4⁺ T cells have the ability to regulate physical reactions (Figure 1G). T cell-derived IFN- γ has also been shown to be involved in regulating neuronal connection and social behavior (Filiano et al., 2016). Without additional stimulation, the splenic CD4⁺ T cells from ES mice

exhibited a significant reduction in IFN- γ expression compared to that in NT mice (Figure S1G). However, serum IFN- γ showed no difference compared to that in NT mice, due to the increased total cell number (Figure S1H).

To elucidate whether the pathological CD4⁺ T cells in anxiety exercise their functions in a manner dependent on their activation, we compared the abilities of naive and effector CD4⁺ T cells to induce anxiety symptoms by adoptive transfer into *Rag1*^{-/-} mice. In addition to naive CD4⁺ T cells, we added two effector control groups including the Effector-L (from the same mice) and Effector-H groups (the same cell number). Although the transferred naive and effector CD4⁺ T cells displayed similar activation features (Figure S1I), naive CD4⁺ T cells triggered a more severe anxiety than did those from the two effector control groups (Figure 1H). Consequently, these data implied an important role for CD4⁺ T cells in stress-induced anxiety independent of their activation status.

Stress Induces Mitochondrial Fission in Peripheral CD4⁺ T Cells

To examine the distinct ability of CD4⁺ and CD8⁺ T cells to drive anxiety, we analyzed the transcriptome of naive ES-induced CD4⁺ and CD8⁺ T cells by RNA sequencing (RNA-seq). Although most of the genes in ES CD4⁺ T cells were similar to those in the other three groups (Figure 2A and Table S1), 128 specifically differentially expressed genes (DEGs) were identified in ES-induced CD4⁺ T cells (Figures 2B and 2C). Gene ontology (GO) analysis revealed that a large number of these DEGs encoded mitochondrial proteins (Figure 2D). Additionally, both ES- and RS-treated naive CD4⁺ T cells exhibited severely reduced levels of glycolysis (Figure 2E) and oxidative phosphorylation (OXPHOS) (Figure 2F), as measured by the extracellular acidification rate (ECAR) and oxygen consumption rate (OCR), respectively. These data implied that stress affected the structure of mitochondria, which profoundly influences the biogenesis and function of mitochondria (Wai and Langer, 2016; Zhan et al., 2013). Confocal microscopy images demonstrated that ES-treated naive CD4⁺ T cells predominantly exhibited punctate mitochondria (Figure 2G). Consistently, compared to those from healthy donors, naive CD4⁺ T cells from the patients with anxiety also displayed severe mitochondrial division (Figure S2A). Immunoblotting (IB) further revealed that the outer membrane proteins that mediated mitochondrial fusion, including MFN2 and MIGA2, were significantly reduced in ES-treated naive CD4⁺ T cells (Figure 2H and Figure S2B). Collectively, these data suggest that CD4⁺ T cells under stress exhibit abnormal mitochondrial morphology and metabolic dysfunction.

Various neurotransmitters and hormones including dopamine, cortisol, GABA, adrenaline, L-glutamic acid and serotonin have been proven to be associated with the onset of anxiety. Surprisingly, these critical molecules in the serum did not display any consistent trends of changes between the ES- and RS-induced anxiety models (Figure S2C). Adrenal glucocorticoids appear to weaken inflammation and T-cell proliferation. Although injection of prednisone, a glucocorticoid, triggered anxiety-like behavior, CD4⁺ T-cell depletion had no effect on these anxiety symptoms (Figure S2D), suggesting

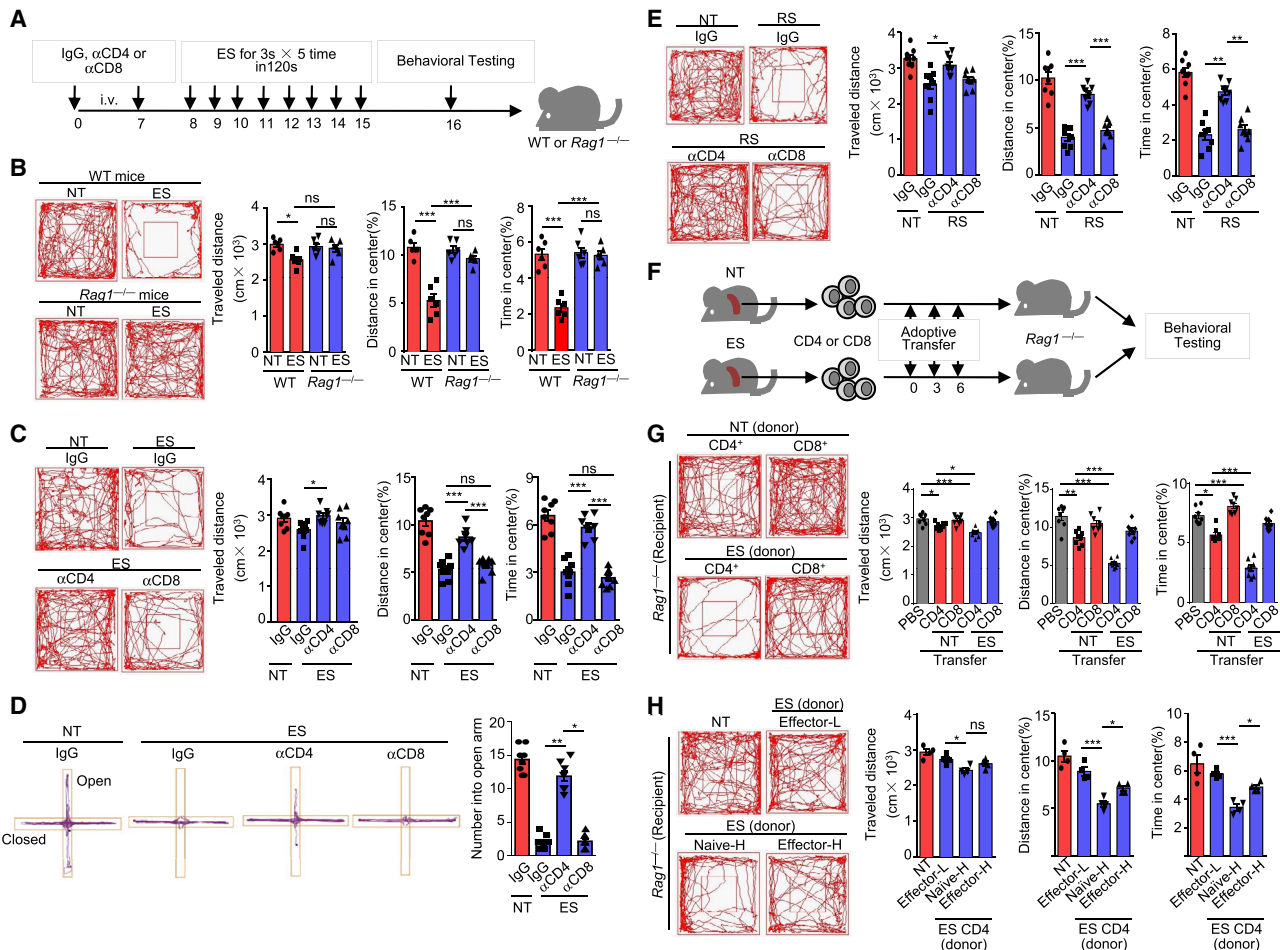


Figure 1. CD4⁺ T Cells Play an Essential Role in Stress-Induced Anxiety-like Behavior

(A–D) Schematic of experimental design. ES, electronic foot shock; NT, nontreated; i.v., intraperitoneal injection. The treatment with indicated antibodies are only for (C) and (E).

(B) Representative tracks of wild-type (WT) or $Rag1^{-/-}$ mice in open-field test (OFT) ($n = 6$) on day 8 after inducing ES model, as well as travel distance, percentage of distance in center area and percentage of time spent in center.

(C) NT- and ES-treated mice were pretreated with indicated antibodies (500 μ g/mice) twice. Representative tracks and statistic results in OFT were measured on day 16 from the first injection ($n = 8$).

(D) Representative tracks and statistic results in elevated plus-maze (EPM) of NT and ES mice described as (C) on day 16 ($n = 8$).

(E) OFT results for restraint stress (RS)-induced anxious mice pretreated with distinct antibodies ($n = 8$).

(F) Schematic of experimental design for T cell adoptively transfer-induced anxiety model.

(G) $Rag1^{-/-}$ mice were i.v. adoptively transferred with 5×10^6 CD4⁺ or CD8⁺ T cells isolated from NT or ES-treated mice (donor) for every three days. The anxiety-like behavior of recipient $Rag1^{-/-}$ mice was evaluated by OFT on day 8 ($n = 8$).

(H) $Rag1^{-/-}$ mice were adoptively transferred with 1.8×10^6 effector (CD4⁺CD44^{hi}CD62L^{lo}, Effect-L), 6×10^6 naive (CD4⁺CD44^{lo}CD62L^{hi}, Naive-H) and 6×10^6 effector (CD4⁺CD44^{hi}CD62L^{lo}, Effect-H) CD4⁺ T cells isolated from ES-treated mice for every three day. Eight days later, the anxiety-like behavior of these recipient $Rag1^{-/-}$ mice was evaluated by OFT ($n = 4$).

All data are representative of at least three independent experiments. Data are represented as means \pm SEM. The significance of difference in (B–E) and (G–H) was determined by Dunnett's multiple comparisons test (Dunnett's Test). ns, no significance; * $p < 0.05$; ** $p < 0.01$; *** $p < 0.005$.

that glucocorticoids may not be involved in CD4⁺ T-cell-induced anxiety. Several findings have demonstrated that depressive animals exhibit increases in omega-6 fatty acids and arachidonic acid (AA) in the brain. AA is known to be a critical component of the inflammatory process via metabolism into leukotriene B4 (LTB4) and prostaglandin (PG) E2, which may further act on peripheral lymphocytes. Of all AA metabolites, only LTB4, PGB1, and 15- δ - Δ 12,14-PGJ2 (15-d-PGJ2)

showed a consistent increase by LC-MS (Figure 2I). In contrast to PGB1, LTB4 administration caused a severe anxiety-like behavior, which was restored by CD4⁺ T cell removal (Figure 2J). Although 15-d-PGJ2 also led to mild anxiety symptoms, CD4⁺ T cells were not involved in this process (Figure 2J). LTB4 significantly promoted mitochondrial fission *in vitro* (Figure 2K) and reduced MFN-2 and MIGA2 expression in naive CD4⁺ T cells (Figure 2L). In summary, stress-induced LTB4

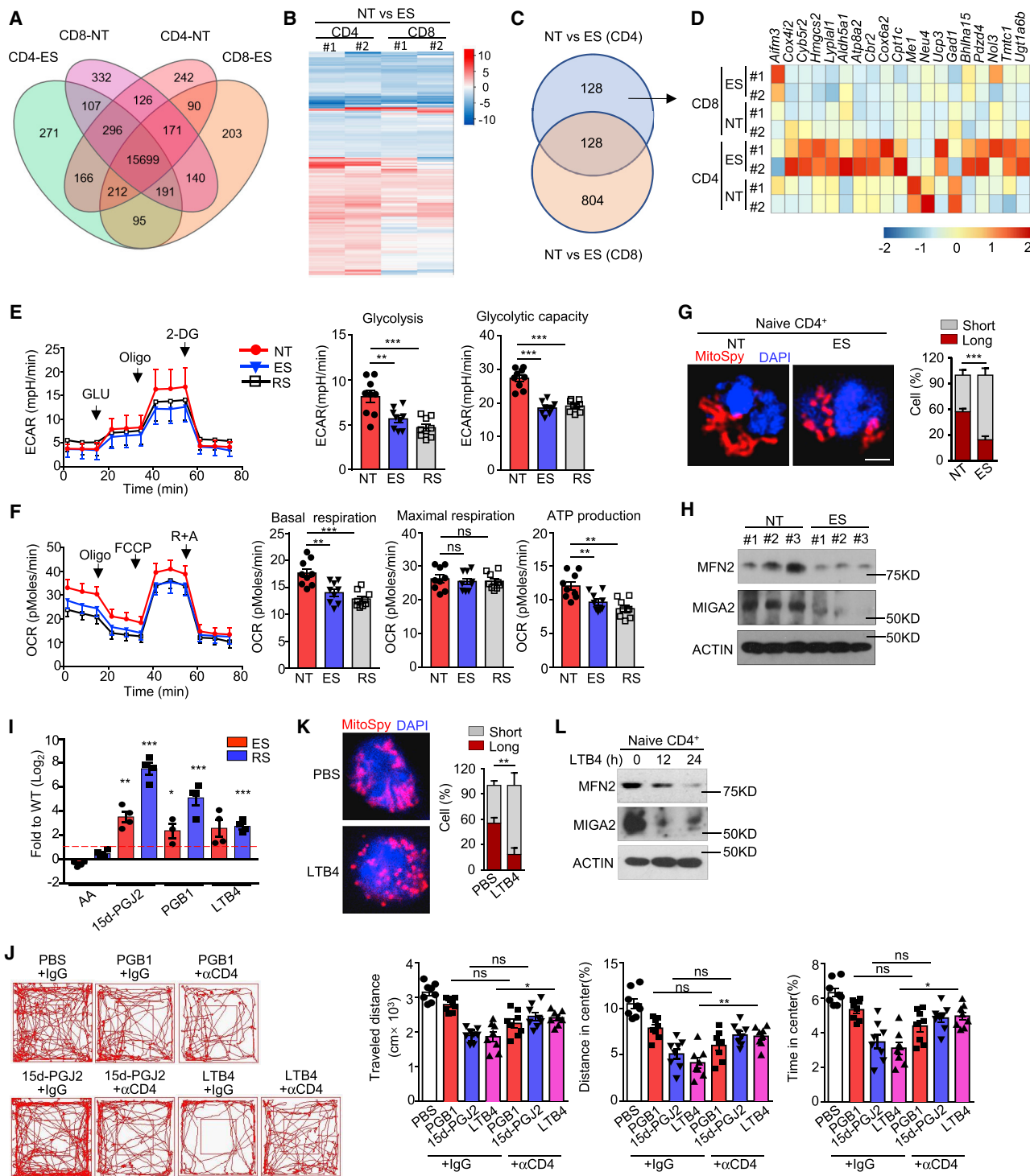


Figure 2. Stress Causes Metabolic Disorder and Mitochondrial Fission in CD4⁺ T Cells

(A) Venn diagram summarizing the expression of genes in naive T lymphocytes isolated from the spleens of NT- or ES-treated mice, as determined by RNA-seq data.

(B) Heatmap showing the differentially expressed genes (DEGs) in T lymphocytes between NT- and ES-treated mice. The DEGs were identified with a fold change of ES/NT > 2.0 or < 0.5.

(C) Comparison of the number of DEGs and gene ontology (GO) analysis of 128 specific DEGs in CD4⁺ T cells.

(D) Heatmap showing the expression of the DEGs encoding mitochondrial proteins.

(legend continued on next page)

triggers mitochondrial fission in peripheral CD4⁺ T cells and the onset of anxiety, although the underlying mechanism remains to be further investigated.

CD4⁺ T Cells with Diverse Mitochondria Cause Severe Anxiety-like Symptoms

To confirm the relationship between the mitochondrial morphology of T cells and anxious behavior, we generated *Mitoguardin 2* KO (*Miga2*^{-/-}) mice and observed highly fragmented mitochondria in naive CD4⁺ T cells (Figure 3A). Ultrastructural analysis with electron microscopy (EM) further confirmed many small, diverse mitochondria dispersed in the cytoplasm of *Miga2*^{-/-} naive CD4⁺ T cells (Figure 3B). Interestingly, *Miga2*-deficient mice displayed decreased locomotor activity and spent much less time in the center than their WT littermates in the OFT (Figure 3C). Consistently, these *Miga2*-deficient mice were obviously afraid to enter into the open arms in the EPM test (Figure 3D). In the dark-light transition assay, *Miga2*-deficient mice exhibited fewer transitions from the dark zone to the light zone and spent less time in the light zone than WT mice (Figure S3A). Moreover, *Miga2*-deficient mice stopped struggling earlier in the tail suspension test (Figure S3B) and exhibited less social motivation and curiosity (Figure S3C), suggesting that these mice also have severe depression.

Similar to the data in the ES stress model, depletion of CD4⁺, but not CD8⁺, T cells restored the anxiety symptoms caused by continuous mitochondrial division (Figure 3E). Although inflammatory microglia lead to depression and anxiety by inhibiting the release of dopamine (Li et al., 2014; McKim et al., 2018; Wang et al., 2018; Wohleb et al., 2011), microglia were not involved in the onset of anxiety caused by *Miga2* deficiency, as revealed by selectively eliminating myeloid cells by liposomal clodronate (LCCA), PLX3397, or BLZ945 (Figure 3E). Recipient *Rag1*^{-/-} mice adoptively transferred with *Miga2*-deficient naive CD4⁺ T cells further confirmed the essential roles of these cells in anxiety (Figure 3F). Both integrin VLA-4 and CD6 are expressed on the T cell surface and allow these cells to penetrate the blood brain barrier (BBB) (Engelhardt et al., 2017; Lécuyer et al., 2017; Li et al., 2017; Ransohoff and Engelhardt, 2012; Theien et al., 2001; Vajkoczy et al., 2001). To clarify whether these “anxious” CD4⁺ T cells function in the CNS, we treated *Miga2*^{-/-} mice with VLA-4 or CD6 neutralizing antibodies, which disrupt T cell migration into the CNS. Surprisingly,

neither the VLA-4 nor CD6 antibody had any effect on anxiety symptoms in *Miga2*-deficient mice (Figure S3D). All of these data indicate that *Miga2* deficiency-induced anxiety is independent of pathological CD4⁺ T cell migration into the brain.

To further clarify the particular function of mitochondrial fission in peripheral CD4⁺ T cells, we generated *Miga2*^{TKO} T cell-conditional knockout (KO) (*Miga2*^{TKO}) mice. In contrast to another mitochondrial fusion protein *Opa1*, which is required for memory T cell characteristics (Buck et al., 2016), *Miga2*-deficient T cells did not show any obvious abnormalities in the development and homeostasis of T lymphocytes (Figures S3E and S3F). *Miga2*^{TKO} mice also displayed comparable sensitivities in models of experimental autoimmune encephalomyelitis (EAE) (Figure S3G), as revealed by comparable clinical scores, levels of immune cell infiltration in the CNS, and proliferative capacity (Figures S3H and S3I). Nevertheless, *Miga2*^{TKO} mice still displayed anxiety-like behavior similar to that of *Miga2*^{-/-} mice (Figure 3G). Furthermore, *Miga2*^{TKO} mice exhibited normal extinction of fear memory in the continuous EPM test (Figure 3H), indicating that *Miga2*-deficient CD4⁺ T cells have no effect on normal learning and memory. To eliminate a particular function of the MIGA2 protein in anxiety, we generated *Mfn1* and *Mfn2* T cell-conditional double KO (*Mfn1/2*^{TKO}) mice. Behavioral assessment indicated that the mice lacking *Mfn1/2* in T cells also exhibited anxiety-like behavior compared to their WT littermates (Figure 3I), suggesting that anxious behavior is promoted by the morphological disorder of mitochondria rather than by a specific function of certain mitochondrial proteins in CD4⁺ T cells.

Continuous Mitochondrial Fission in T Cells Causes a Systemic Purine Metabolism Disorder

Mitochondria morphology has been intimately linked to metabolic regulation across cell types and tissues (Mishra and Chan, 2016; Wai and Langer, 2016). Consistently, partial least-squares discrimination analysis (PLS-DA) revealed that the metabolomic profile of *Miga2*^{TKO} mice was significantly different from that of their WT littermates (Figure 4A and Table S2). Some amino acids, including Trp and glutamate (Glu), account for the majority of excitatory and inhibitory neurotransmitters in the nervous system. Although various amino acids were upregulated in the serum of *Miga2*^{TKO} mice (Figure S4A), these neurotransmitter amino acids and their derivatives were not included (Figure S4B).

(E–F) Mitochondrial fitness tests were used to compare the oxygen consumption rate (OCR) (E) and extracellular acidification rate (ECAR) (F) of naive CD4⁺ T cells isolated from NT- or ES-treated mice (n = 9). The statistical results are presented as a bar graph (right).

(G) The mitochondrial morphology of naive CD4⁺ T cells from NT- or ES-treated mice was visualized using Mitospot™ Orange CMTMRos staining. Representative confocal images are shown, as well as length quantification with 50 cells by Image-Pro. long, brown > 7 μm and short, gray < 7 μm. Bar, 5 μm.

(H) Immuno-blot (IB) analyses of indicated proteins in splenic naive CD4⁺ T cells. #1, repeat 1; #2, repeat 2; #3, repeat 3. See also Figure S2B for the quantification of the relative density of these IB assays.

(I) LC-MS of indicated metabolites in the serum of ES-treated and RS-treated mice, presented relative to the mean value for NT mice (n = 4).

(J) WT mice were i.p. injected with indicated metabolites with αCD4 twice every three days. Anxiety-like behavior of these mice was assessed in OFT on day 8 (n = 8).

(K) Naive CD4⁺ T cells were isolated by FACS sorter and stimulated with leukotriene B4 (LTB4) for 24 h. Mitochondrial morphology was visualized and quantified with 50 cells.

(L) IB analyses of the MFN2 and MIGA2 protein levels in naive CD4⁺ T cells stimulated with LTB4.

All data are representative of at least three independent experiments. Data are represented as means ± SEM. The significances of difference in (E), (F), and (J) were determined by Dunnett's Test, and others were determined by two-tailed Student's t test (t test). *p < 0.05; **p < 0.01; ***p < 0.005.

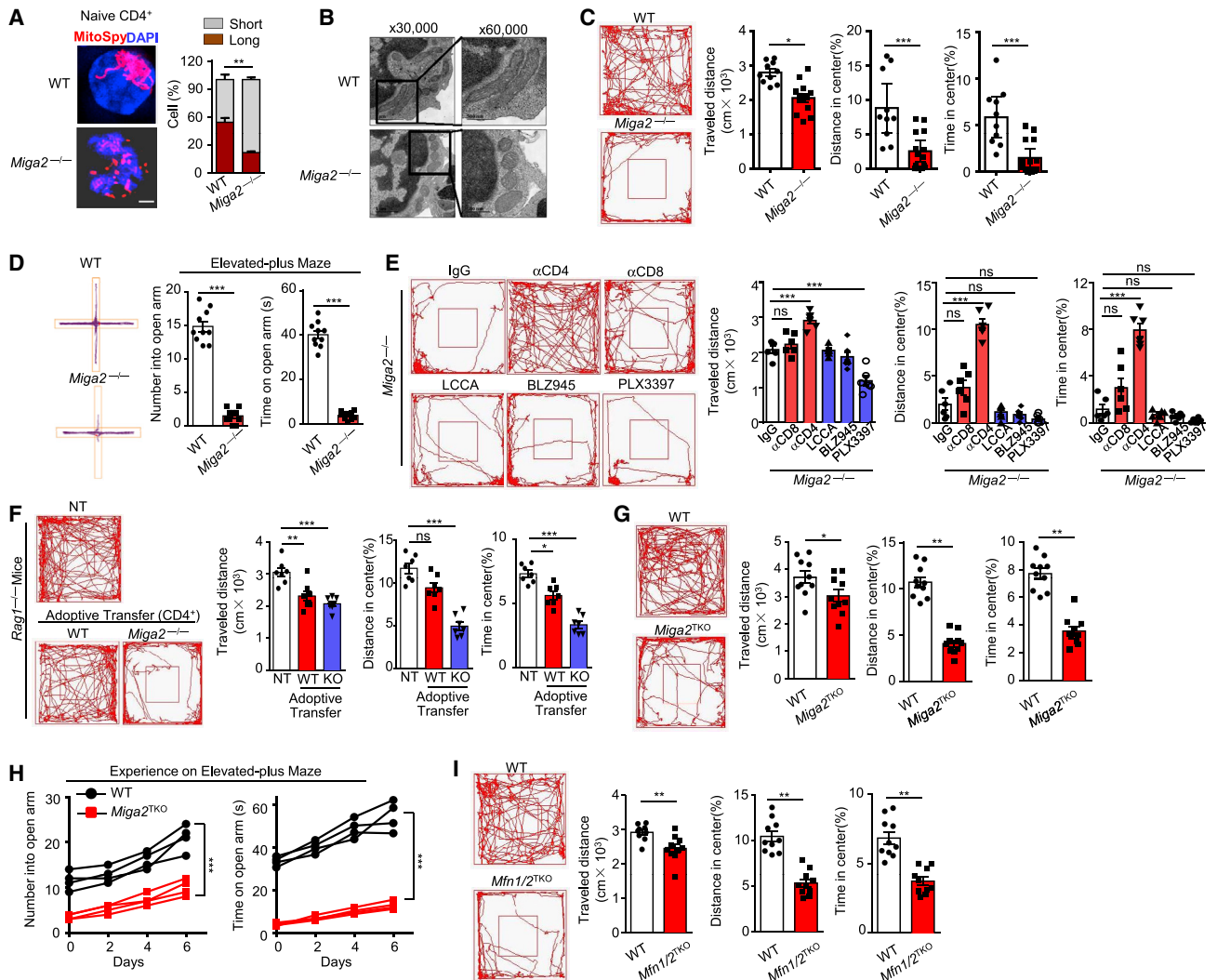


Figure 3. Sustained Mitochondrial Fission in CD4⁺ T Cells Induces the Anxiety-like Behavior

(A) Mitochondrial morphology of splenic naive CD4⁺ T cells isolated from 6-to-8-week-old WT or Miga2^{-/-} mice was visualized and quantified with 50 cells.

(B) Mitochondrial morphology of WT and Miga2^{-/-} CD4⁺ T cells was analyzed by EM (scale bar, 500 nm or 1 μm).

(C) Representative tracks of WT and Miga2^{-/-} mice in OFT (left, n = 10).

(D) Representative tracks in the EPM (n = 10). The number of entries into the open arms and the time spent in the open arms are presented as bar graphs (right).

(E) Some of WT and Miga2^{-/-} mice were i.v. injected with distinct antibodies on days 0 and 7, and together i.v. injected with liposomal clodronate (LCCA, 70 mg/kg) or i.p. injected with PLX3397 (50 mg/kg) or BLZ945 (200 mg/kg) on days 0, 2, 4, and 6. The anxiety-like behavior of these mice were then evaluated in OFT on day 8 (n = 6).

(F) Rag1^{-/-} mice were adoptively transferred with 5 × 10⁶ WT or Miga2^{-/-} splenic CD4⁺ T cells every three days. Six days later, the anxiety-like behavior of recipient Rag1^{-/-} mice was evaluated in OFT (n = 7).

(G) OFT results for 6-to-8-week-old Miga2^{TKO} mice with their littermates (n = 10).

(H) The WT and Miga2^{TKO} mice were continuously subjected to EPM each day and measured for their responsive experience in every other day (n = 4).

(I) Representative tracks of 6-to-8-week-old WT and Mfn1/2^{TKO} mice in the OFT (n = 10). All data are representative of at least three independent experiments.

Data are represented as means ± SEM. The significances of differences in (E) and (F) were determined by Dunnett's test, and others were determined by t test. *p < 0.05; **p < 0.01; ***p < 0.005.

Hierarchical clustering and KEGG analyses indicated that the differential metabolites in Miga2^{TKO} mice were mainly enriched in purine metabolism (Figures 4B and 4C). Most of the purines and their derivatives including adenine, hypoxanthine, and xanthine were 10 to 100 times more abundant in Miga2^{TKO} mice than in their WT littermates (Figure 4D). Interestingly,

xanthine mainly accumulated in the brain but was markedly decreased in the peripheral immune organs (Figure S4C). After the removal of CD4⁺ T cells, the serum concentration of xanthine in Miga2^{TKO} mice was significantly decreased (Figure 4E). Current clinical evidence has revealed that patients with depression have an increased level of xanthine compared with that of healthy

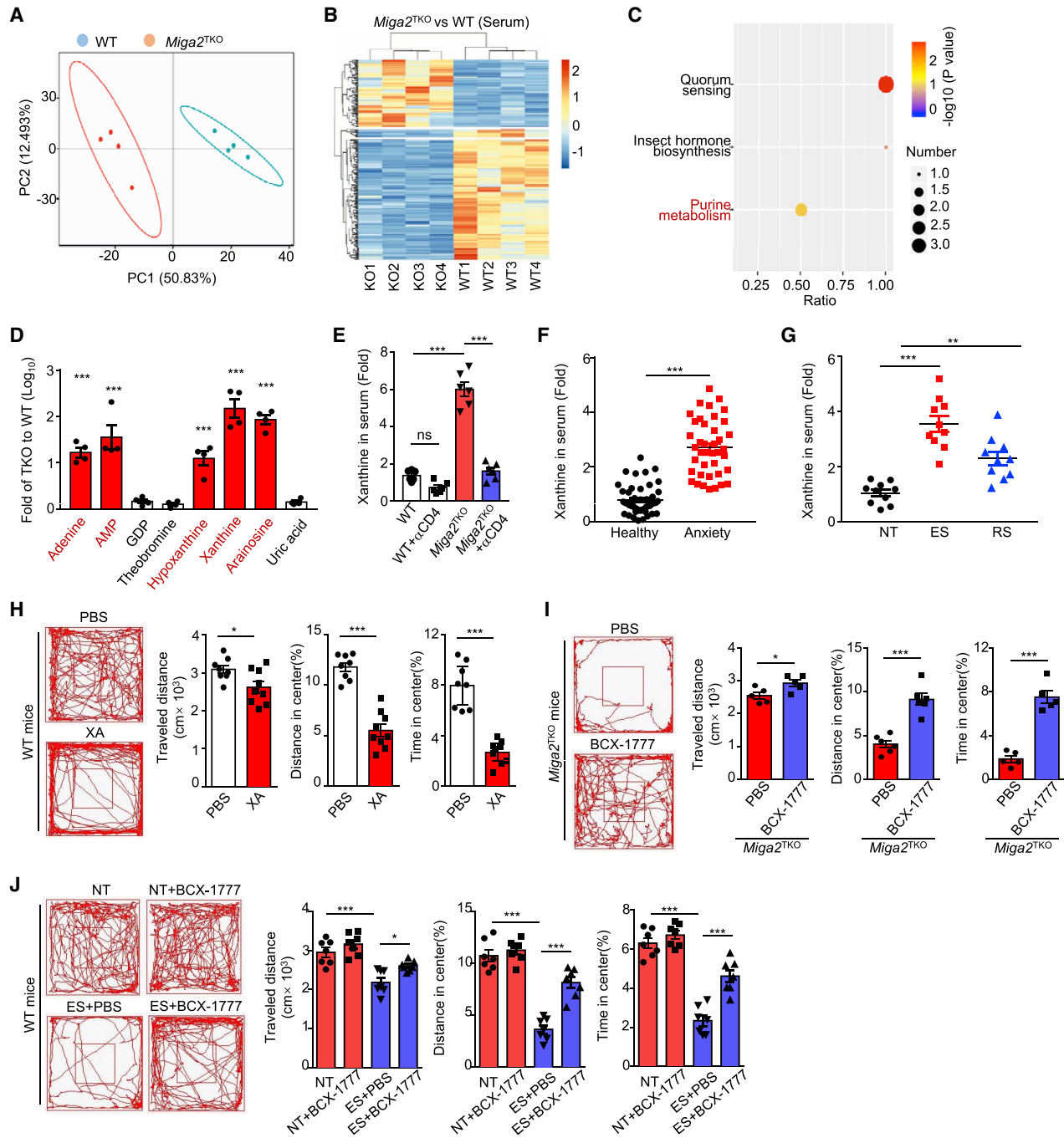


Figure 4. Mitochondrial Fission in CD4⁺ T Cells Leads to a Systemic Increase in Serum Purines

(A) Partial Least-squares discrimination analysis (PLS-DA) of the serum metabolome of WT and Miga^{2TKO} mice (n = 4). Each symbol represents the data of an individual mouse.

(B) Heatmap showing differential metabolic production (DMP) in the serum of WT and Miga^{2TKO} mice. The DMPs were identified with a fold change of Miga^{2TKO}/WT > 2.0 or < 0.5.

(C) KEGG analysis of these DMPs-enriched biological processes.

(D) Purine nucleotides and their derivatives in the serum were measured by PLS-DA and presented as the ratio of the abundance in Miga^{2TKO} mice to those in WT mice (n = 4).

(E) Xanthine in the serum of CD4⁺ T cell-depleting Miga^{2TKO} mice was measured by ELISA. The relative fold is to serum xanthine concentration of WT control.

(F) Dot plots showing the relative fold of xanthine in the serum of the patients with anxiety (n = 40) to those in healthy donors (n = 46).

(G) ELISA assay of the relative fold of xanthine in the serum of NT-, ES-, and RS-treated mice (n = 10).

(legend continued on next page)

controls (Ali-Sisto et al., 2016). We also found that serum xanthine was significantly higher in patients with anxiety (Figure 4F). Increased abundance of serum xanthine was also observed in two rodent anxiety models (Figure 4G) and the recipient *Rag1*^{-/-} mice adoptively transferred with ES CD4⁺ T cells (Figure S4D). Similar to the observation that anxiety is mainly induced by naïve T cells in Figure 1H, naïve CD4⁺ T cells produced a higher level of xanthine than effector T cells (Figure S4E).

To verify the direct link between excessive levels of purines and anxiety symptoms, we intraperitoneally (i.p.) injected synthetic xanthine or adenosine into WT mice. Surprisingly, xanthine, adenine, and adenine arabinoside monophosphate (Ara-AMP) all had the ability to trigger anxiety-like behavior (Figure 4H and Figure S4F). Previous reports have revealed opposite effects of adenine and xanthine on the activity of neurons (Phillis and Wu, 1982). Thus, we measured c-FOS expression on neurons, which indicates their activation after xanthine or adenosine administration. Similar to in *Miga2*^{-/-} mice, xanthine treatment caused more c-FOS expression on the neurons than did PBS treatment. Oppositely, adenine led to a reduction in c-FOS⁺ neurons, which could be reversed by xanthine coinjection (Figure S4G). Therefore, xanthine plays a more dominant role when the microenvironment contains both of these purines. BCX-1777, as a purine nucleoside phosphorylase (PNP) inhibitor, has been proven to be an efficient inhibitor of purine metabolism (Li et al., 1999; Miles et al., 1998). BCX-1777 treatment significantly reduced the anxiety symptoms in *Miga2*^{TKO} and ES mice (Figures 4I and 4J) and significantly decreased the serum concentration of xanthine (Figure S4H). In summary, excessive xanthine caused by pathological CD4⁺ T cells plays a critical role in the onset of anxiety.

Xanthine Directly Acts on Oligodendrocytes in the Left Amygdala

A number of studies have suggested that the amygdala plays a critical role in generating fear and persistent anxiety (Davis, 1992; Shackman and Fox, 2016; Thomas et al., 2001). The left amygdala has been linked to social anxiety, compulsive disorders, and posttraumatic stress as well as to general anxiety (Phelps et al., 2001). Histological analysis of *Miga2*^{TKO} mice revealed that the left amygdala of *Miga2*^{TKO} mice was significantly larger and exhibited higher numbers of nonneuronal cells than the right amygdala or the amygdala of the WT control (Figure 5A and Figures S5A and S5B). The left amygdala of xanthine-treated mice displayed a pathological phenotype similar to that of *Miga2*^{TKO} mice (Figure S5C). To clarify the pathological mechanism in the amygdala, we performed single-cell RNA sequencing (scRNA-seq) by using the 10x Genomics platform in an unbiased manner (Figure S5D and Table S3). Approximately 3,000 cells passed quality control, and unsupervised clustering revealed nine clusters, which we visualized with t-distributed stochastic

neighbor embedding (tSNE) (Figure S5E). We defined each population with multiple specific genes and highlighted three markers for each subset (Figure 5C). Adenine and xanthine initiate their physiological functions through four receptor subtypes, namely A1, A2A, A2B, and A3. Interestingly, the scRNA-seq data revealed that A1 is mainly expressed in oligodendrocytes and oligodendrocyte progenitor cells (OPCs), while A2B and A3 are distributed in astrocytes and microglia, respectively (Figure 5D and Table S3). FACS immunofluorescence (IF) analysis further confirmed that A1 expression was largely distributed in oligodendrocytes, but no expression of A2A, A2B, or A3 was detected (Figures 5E–5F and Figure S5F). Due to the defect of adenosine receptors on neurons, we next analyzed the transcriptome of each nonneuronal cell in the amygdala of WT-, *Miga2*^{-/-}, and α CD4-treated *Miga2*^{-/-} mice (Table S4). Both scRNA-seq and FACS analysis indicated a significantly increased percentage of oligodendrocytes in *Miga2*^{-/-} mice, which could be reversed by depleting CD4⁺ T cells (Figures 5G and 5H). Furthermore, more A1⁺ oligodendrocytes were observed in *Miga2*^{-/-} mice but not in those treated with α CD4 (Figure 5F and Figure S5G). Consistently, only DEGs in oligodendrocytes were largely restored by removing CD4⁺ T cells in *Miga2*^{-/-} mice (Figure S5H). KEGG analysis showed that these DEGs in oligodendrocytes were mainly enriched in the purine metabolic process and mitotic cell cycle process (Figure S5I). As a pathogenic factor, xanthine caused a significant increase in DNA synthesis and the cell cycle in oligodendrocytes, as measured by BrdU incorporation assays, while adenine had a significant opposite effect (Figure S5J). Therefore, these data suggest that xanthine triggers the proliferation of oligodendrocytes directly.

Previous evidence has revealed that xanthine acts on A1 receptors and promotes the activity of protein kinase A (PKA)/cAMP (Darashchonak et al., 2014). Consistently, the intense bands of phospho-PKA substrates indicated that the PKA/cAMP pathway was clearly activated in oligodendrocytes of *Miga2*^{-/-} mice and was downregulated by depleting CD4⁺ T cells (Figure S5K). As the only detectable adenosine receptor, A1 in oligodendrocytes was further specifically knocked down by injecting an adeno-associated virus (AAV) expressing myelin basic protein (MBP) promoter-driven *AdorA1* shRNA-GFP (AAV-MBP-sh*AdorA1*-GFP) into the left amygdala (Figure 5I). In parallel, an AAV expressing MBP promoter-driven non-silencing shRNA (AAV-MBP-NCshRNA-GFP) was used as a negative control (Figure 5I). Two weeks later, FACS analysis suggested a strong co-expression of GFP and MOG signals in the left amygdala (Figure 5J), indicating specific expression of *AdorA1* shRNA in oligodendrocytes. Without the A1 receptor in oligodendrocytes, *Miga2*-deficient mice no longer displayed anxiety-like symptoms (Figure 5K). In summary, the excessive xanthine caused by *Miga2*^{-/-} T cells acts on oligodendrocytes

(H) WT mice were i.p. injected with xanthine (500mg/kg) once every three days. Anxiety-like behavior of these mice was assessed in OFT on day 8 (n = 8).

(I) *Miga2*^{TKO} mice were i.p. injected with BCX-1777 (20mg/kg) once every three days. Anxiety-like behavior was evaluated in OFT as above on day 8 (n = 5).

(J) ES-treated mice were i.p. injected with PBS or BCX-1777 (20mg/kg) every three days. The anxiety-like behavior of these mice was evaluated by OFT on day 8 (n = 7).

All data are representative of at least three independent experiments. Data are represented as means \pm SEM. The significances of differences in (D), (E), (G) and (J) were determined by Dunnett's test, and others were determined by t test. *p < 0.05; **p < 0.005.

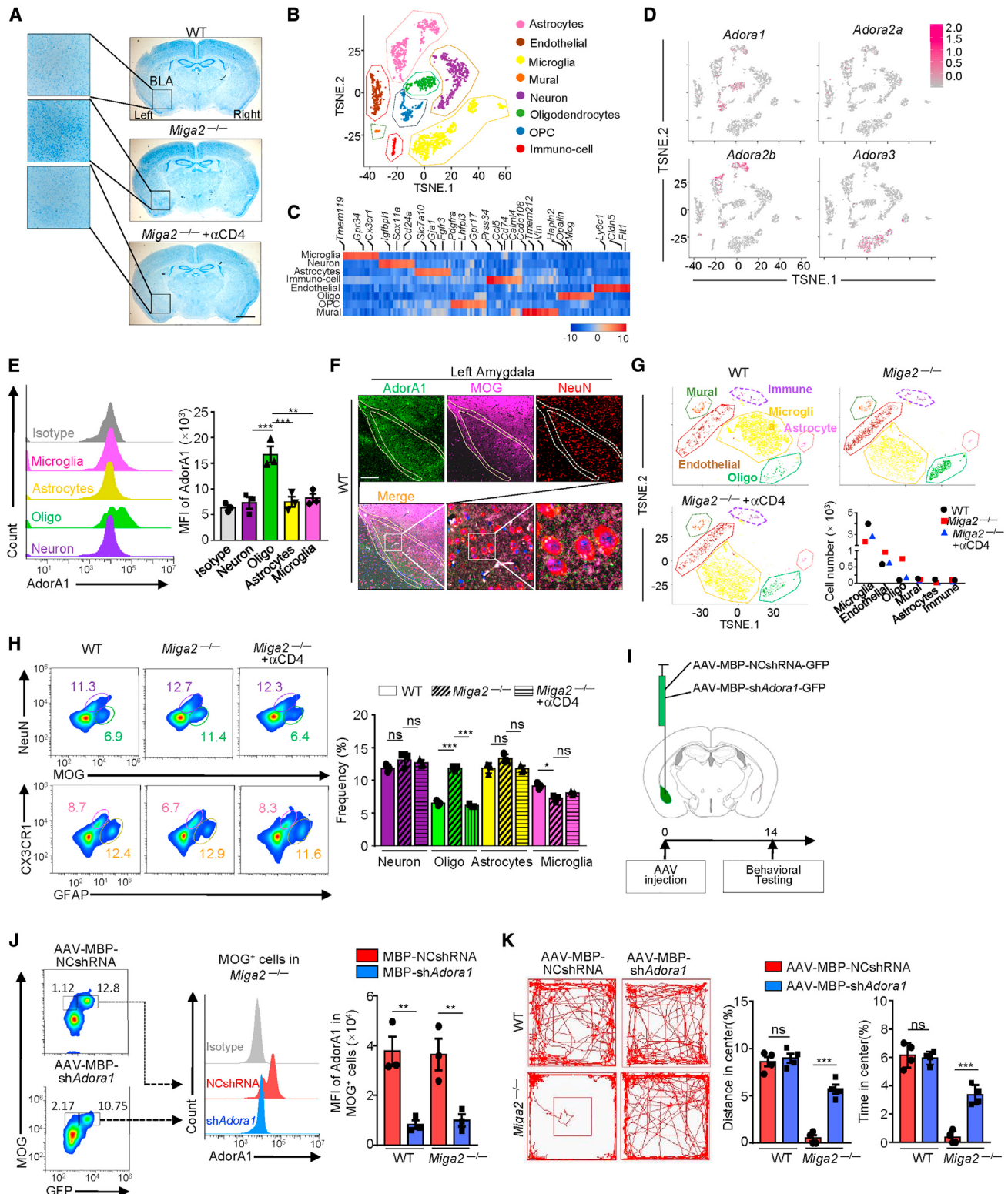


Figure 5. CD4⁺ T Cell-Derived Xanthine Acts on the Oligodendrocytes at the Amygdala via AdorA1

(A) Histological analyses of whole brains were performed by Nissl staining. Scale bar, 100 μm. See also Figure S5B for the statistical results.

(B) tSNE plots of scRNA-seq show unsupervised clusters of cells in the amygdala. 9 major clusters; OPC, oligodendrocyte progenitor cell.

(C) Heatmap of each cluster's expression of the 15 markable DEGs per cluster.

(legend continued on next page)

through the A1 receptor in the left amygdala and promotes anxiety-like behavior.

Mitochondrial Fission Promotes the *de novo* Synthesis of Xanthine in CD4⁺ T Cells

Purine can be synthesized via two distinct pathways: the *de novo* synthesis pathway, the glucose metabolic product 5-phosphoribosyl-1-pyrophosphate (PRPP) provides a backbone to form the purine ring. Similar to ES-treated T cells, *Miga2*-deficient CD4⁺ T cells exhibited markedly reduced activities of OXPHOS and glycolysis (Figure 6A and Figures S6A and S6B). A similar metabolic pattern was observed in CD4⁺ T cells from *Mfn1/2*^{TKO} mice (Figures S6C and S6D). A ¹³C carbon tracing assay further revealed that *Miga2*-deficient naive CD4⁺ T cells had lower glycolysis levels but produced more M+5 ribulose-5-p (R-5-P), CAIR, adenosine, and inosine than the WT naive CD4⁺ T cells (Figures 6B–6C and Table S5), demonstrating that glucose flows to the pentose phosphate pathway (PPP) for *de novo* purine synthesis upon the alteration of mitochondrial morphology from fusion to fission. 2-Deoxy-D-glucose (2-DG) is a glucose analog that inhibits its catabolic pathways including glycolysis, PPP, and *de novo* purine synthesis by inhibiting hexokinase activity. The administration of 2-DG clearly normalized the anxiety-like symptoms and pathological characteristics of the left amygdala in *Miga2*^{TKO} mice (Figures S6E and S6F).

To clarify the underlying mechanism by which mitochondrial morphology regulates purine synthesis, we analyzed the transcriptome of WT and *Miga2*-deficient naive CD4⁺ T cells. *Miga2*-deficient CD4⁺ T cells showed reduced transcription of several critical enzymes related to the glycolytic and fatty acid β-oxidation pathway, but increases in the molecules required for purine synthesis, such as hexokinase 3 (*Hk3*), adenosine deaminase (*Ada*), purine nucleoside phosphorylase 2 (*Pnp2*), and xanthine oxidase/xanthine dehydrogenase (*Xdh*) (Table S6 and Figure 6D). Additionally, qPCR and IB analyses in *Miga2*-deficient naive CD4⁺ T cells confirmed the elevated mRNA and protein levels of these genes (Figures 6E and 6F), which were consistent with the accumulation of the associated metabolites (Figures 4A and 6G).

PNP catalyzes the conversion of inosine and guanosine to hypoxanthine or guanine. Similar to PNP, PNP2 also functions as an enzyme regulating the purine metabolic pathway and xanthine production. Due to its low expression in primary CD4⁺ T cells, we proposed that its deficiency may not lead to

a severe immunodeficiency as *Pnp* deficiency does (Arpaia et al., 2000; Markert, 1991; Stoop et al., 1977). Thus, we generated *Pnp2*^{−/−} mice with CRISPR/CAS9 by targeting exon 2 (Figure 6H and Figure S6G) and verified with qPCR analysis (Figure S6H). Consistent with our hypothesis, *Pnp2*-deficient mice did not exhibit any obvious dysfunction of T lymphocyte development or maturation (Figure S6I) and were thus further crossed with *Miga2*^{−/−} mice to generate *Pnp2*^{−/−}*Miga2*^{−/−} mice. *In vitro*, *Pnp2* deficiency partially normalized the hyper-production of xanthine by *Miga2*^{−/−} T cells (Figure 6I). After adoptive transfer into *Rag1*^{−/−} mice, *Pnp2*^{−/−}*Miga2*^{−/−} CD4⁺ T cells did not induce anxiety symptoms as strong as those induced by *Miga2*^{−/−} CD4⁺ T cells (Figure 6J). Because *Pnp2* depletion cannot completely block the synthesis of xanthine, xanthine in the serum was still moderately increased in the recipient *Rag1*^{−/−} mice transferred with *Pnp2*^{−/−}*Miga2*^{−/−} CD4⁺ T cells (Figure 6K). These results support the conclusion that CD4⁺ T-cell-derived excess xanthine directly causes anxiety-like behavior.

Mitochondrial Fission Leads to Excessive Xanthine by Promoting IRF-1 Accumulation

Interferon regulatory factor-1 (IRF-1), a transcription factor, participates in various cellular processes, including cell proliferation, differentiation, apoptosis, and immunological regulation. Our previous study revealed that constitutive mitochondrial fission promoted the accumulation of IRF-1 in innate immune cells (Gao et al., 2017). We found that the stability of IRF-1 was negatively regulated via monoubiquitination by the carboxyl terminus of hsp70-interacting protein (CHIP), which was degraded by the diverse mitochondria-recruited ubiquitin E3 ligase PARKIN (Gao et al., 2017) (Figure S6J). Similar to macrophages, *Miga2* deficiency also triggered significant aggregation of IRF-1 in CD4⁺ T cells (Figure 7A). Consistently, ES also caused severe accumulation of IRF-1 in CD4⁺ T cells (Figure 7B). Analysis of public data regarding chromatin immunoprecipitation sequencing (ChIP-seq) of macrophages (Langlais et al., 2016) revealed that IRF-1 was enriched in the promoter regions of *Ada*, *Xdh*, and *Pnp2*. Thus, we analyzed the promoter sequence of these three genes and identified several potential IRF-1 binding motifs near the transcription start site (TSS) (Figure 7C). ChIP-qPCR assays further revealed that the accumulated IRF-1 in *Miga2*-deficient CD4⁺ T cells was significantly enriched at certain binding sites in the TSSs of *Ada*, *Pnp2*, and *Xdh* compared to those in WT controls (Figure 7D). We next depleted IRF-1 in *Miga2*-deficient

(D) Dot plots showing the distributed expression of distinct adenosine receptors for each cell cluster on the t-SNE map.

(E) Flow cytometry analysis of AdorA1⁺ expression in each cell-type at the amygdala of WT mice (n = 3). Astrocytes are defined as GFAP⁺; Neurons are defined as NeuN⁺; Oligodendrocytes (Oligo) are defined as MOG⁺; Microglia are defined as CX3CR1⁺.

(F) Representative immunofluorescence images of FITC-AdorA1 (green), APC-MOG (purple), and PE-NeuN (red) staining in sections of the amygdala from 8-week-old WT mice. Scale bar, 10 μm.

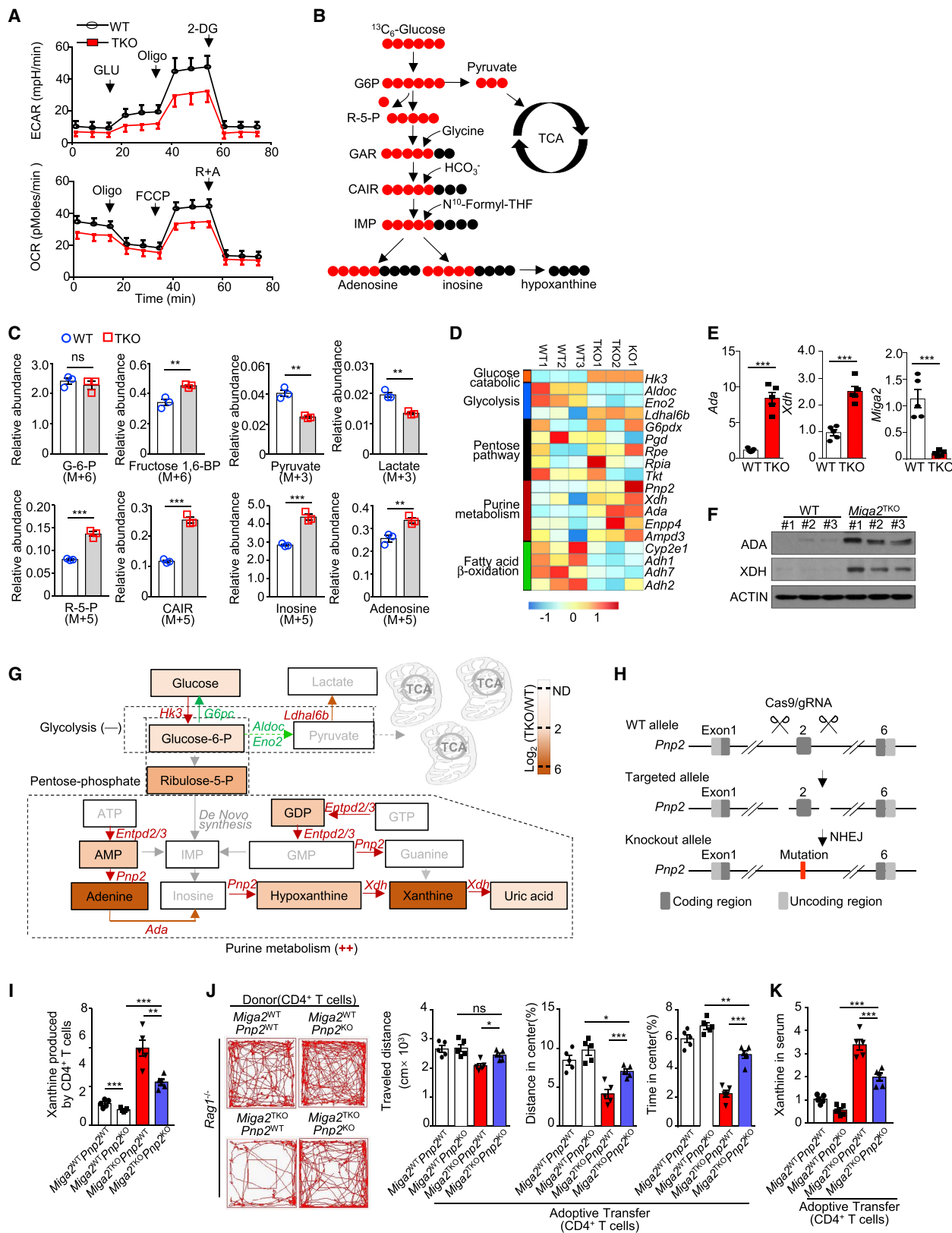
(G–H) tSNE plots of scRNA-seq (G) and flow cytometry (FACS) analysis (H) show unsupervised clustering of non-neuronal cells in the amygdala of 6–8-week-old WT, *Miga2*^{−/−}, and *Miga2*^{−/−} mice treated with αCD4 (n = 3).

(I) Vector structure of the adeno-associated virus (AAV)-AdorA1 shRNA under the control of myelin basic protein (MBP) promoter. The non-silencing shRNA (NCshRNA) was used as a negative control. WT or *Miga2*^{−/−} mice were injected with AAV in the left amygdala.

(J) Two weeks later, FACS analyses of AdorA1 expression on the AAV-infected MOG⁺ oligodendrocytes in the left amygdala.

(K) WT or *Miga2*^{−/−} mice were injected with AAV as described above and evaluated for anxiety-like behavior by the OFT two weeks later.

All data are representative of at least three independent experiments. Data are represented as means ± SEM. The significances of differences in (E), (H), and (K) were determined by t test. ***p < 0.005.



(legend on next page)

CD4⁺ T cells by crossing with *Irf1*^{-/-} mice. IRF-1 deficiency clearly normalized both the mRNA and protein levels of *Ada* and *Xdh* in *Miga2*-deficient CD4⁺ T cells (Figures 7E and 7F). Additionally, the lack of IRF-1 restored most of the anxiety-like phenotypes in *Miga2*^{TKO} mice (Figure 7G). A weak difference remained between *Miga2*^{TKO}*Irf1*^{KO} and *Miga2*^{WT}*Irf1*^{KO} mice indicating that IRF-1 may not be the only factor contributing to T-cell-mediated anxiety-like behavior. Nonetheless, our results suggest that IRF-1 in CD4⁺ T cells plays an essential role in mitochondrial fission-mediated purine synthesis and anxiety symptoms.

DISCUSSION

As early as 1950, Han Selye built up the concept of neuroimmunology and began to explore the crosstalk between immune cells and the nervous system. Over nearly 70 years, the function of the innate immune system in the control of mood and the onset of anxiety has been well established, but the roles of the adaptive immune system have not yet been defined. Some evidences revealed that both *Rag1*^{-/-} and TCR β ^{-/-} δ ^{-/-} mice exhibit attenuated anxiety- and depression-like behavior (Beurel et al., 2013; Clark et al., 2015; Clark et al., 2014; Cushman et al., 2003; Rattazzi et al., 2013; Rilett et al., 2015). In contrast, some other studies showed that lymphocytes from chronically social defeated mice suppressed anxiety in recipient mice (Brachman et al., 2015; Lewitus et al., 2009). These results suggest that the controversial roles of T cells in mood disorders are largely attributed to the lack of sufficient genetic evidence.

Patients with infectious or autoimmune diseases, such as inflammatory bowel disease, displayed excessive T cell proliferation, which led to anxiety-like behavior (Gracie and Ford, 2019; Kipnis, 2016; Naidoo et al., 2015). Mice with T regulatory cell (Treg) deficiency or anti-PD-1 administration exhausted serotonin and 5-hydroxyindoleacetic acid levels in the brain because of excessively proliferative T cells. However, Trp supplementation only partially normalized behavioral symptoms and neurotransmitter levels (Miyajima et al., 2017). Surprisingly, low levels

of inflammation and dysfunction of T cell responses in CS also trigger anxiety-like behavior, implying that T cells trigger anxiety in a nonconventional manner, even without traditional inflammatory characteristics. Here, our study revealed a critical association between peripheral CD4⁺ T cell-derived xanthine and anxiety-like behavior. Miyajima et al. also demonstrated accumulated purines in the sera of anxious mice treated with anti-PD-1 (Miyajima et al., 2017). Thus, it would be interesting to investigate whether xanthine is also involved in inflammation-induced anxiety.

Purine plays an essential role in various physiological processes including the synthesis of nucleic acids, lipid metabolism, and protein glycosylation. Purines are also required for the development and maintenance of mature T lymphocytes. Defects in critical genes in the purine synthesis pathway, including *Ada* and *Pnp*, cause severe immunodeficiency (Arpaia et al., 2000; Markert, 1991; Stoop et al., 1977). However, the major source of purines *in vivo* has not been clearly identified. Our study demonstrated that CD4⁺ T cells from NT mice produced a considerable amount of xanthine. Furthermore, we observed only weakly increased xanthine levels in the sera of recipient mice that were adoptively transferred with *Miga2*^{-/-}*Pnp2*^{-/-} CD4⁺ T cells. These results suggest that the purine required for the maturation and activation of peripheral T cells may be produced by themselves, which may explain why the *Rag1*^{-/-} mice that received excessive NT CD4⁺ T cells also exhibited moderate anxiety.

In summary, our data establish peripheral CD4⁺ T cells as pivotal mediators of stress-induced mood disorders. In the future, it will be interesting to clarify whether a specific CD4⁺ T cell subpopulation regulates emotions and behavior in anxious patients. It is also important to clarify the mechanism by which LTB4 promotes the mitochondrial morphology of CD4⁺ T cells. Taken together, our results provide insights into the physiological function of adaptive immunity in neurodevelopment and neuropsychiatric disorders. We believe our findings have profound implications for developing a valuable therapeutic approach for various psychiatric and metabolic diseases.

Figure 6. Mitochondrial Fission Promotes Purine de novo Synthesis Pathway in CD4⁺ T Cells

- (A) Mitochondrial fitness tests were used to compare the OCR and ECAR of splenic CD4⁺ T cells ($n = 9$).
 - (B) Schematic diagram of the conversion of ¹³C-glucose into purine metabolism and the tricarboxylic acid (TCA) cycle.
 - (C) Naive splenic CD4⁺ T cells were cultured in glucose-free medium for 6 h and then incubated with ¹³C-glucose for 24 h. LC-MS was performed for M+3-, M+5-, and M+6-labeled metabolic productions.
 - (D) The expressions of selective regulators for distinct metabolic processes in naive CD4⁺ T cells were analyzed by RNAseq and presented by heatmap.
 - (E) The mRNA of indicated genes naive CD4⁺ T cells from WT and *Miga2*^{TKO} mice were monitored by qRT-PCR ($n = 5$). These qPCR data are presented as fold change relative to the Actb mRNA level and normalized by Bio-Rad CFX Manager 3.1.
 - (F) The protein levels of ADA and XDH in the CD4⁺ T cells described as (E) were measured by IB.
 - (G) Schematic showing purine metabolic pathways, listing representative enzymes and metabolic products, color-coded based on fold change. The genes in red characters were upregulated; those in green characters were downregulated.
 - (H) Schematic diagram of *Pnp2* knockout strategy.
 - (I) Naive CD4⁺ T cells were isolated from the indicated mice. These CD4⁺ T cells were cultured in glucose-free medium for 6 h and then incubated with glucose (2mg/mL) for another 24 h. Xanthine in the supernatant was measured by ELISA. The relative fold change is normalized to serum xanthine in the *Miga2*^{WT}*Pnp2*^{WT} group.
 - (J) *Rag1*^{-/-} mice were adoptively transferred with 5×10^6 CD4⁺ T cells as indicated every other day. Six days later, the anxiety-like behavior of these *Rag1*^{-/-} mice was evaluated by OFT ($n = 5$).
 - (K) Xanthine in the serum of above mice was measured by ELISA.
- All data are representative of at least three independent experiments. Data are represented as means \pm SEM. The significances of difference in (I–K) were determined by Dunnett's test, and others were determined by t test. * $p < 0.05$; ** $p < 0.01$; *** $p < 0.005$.

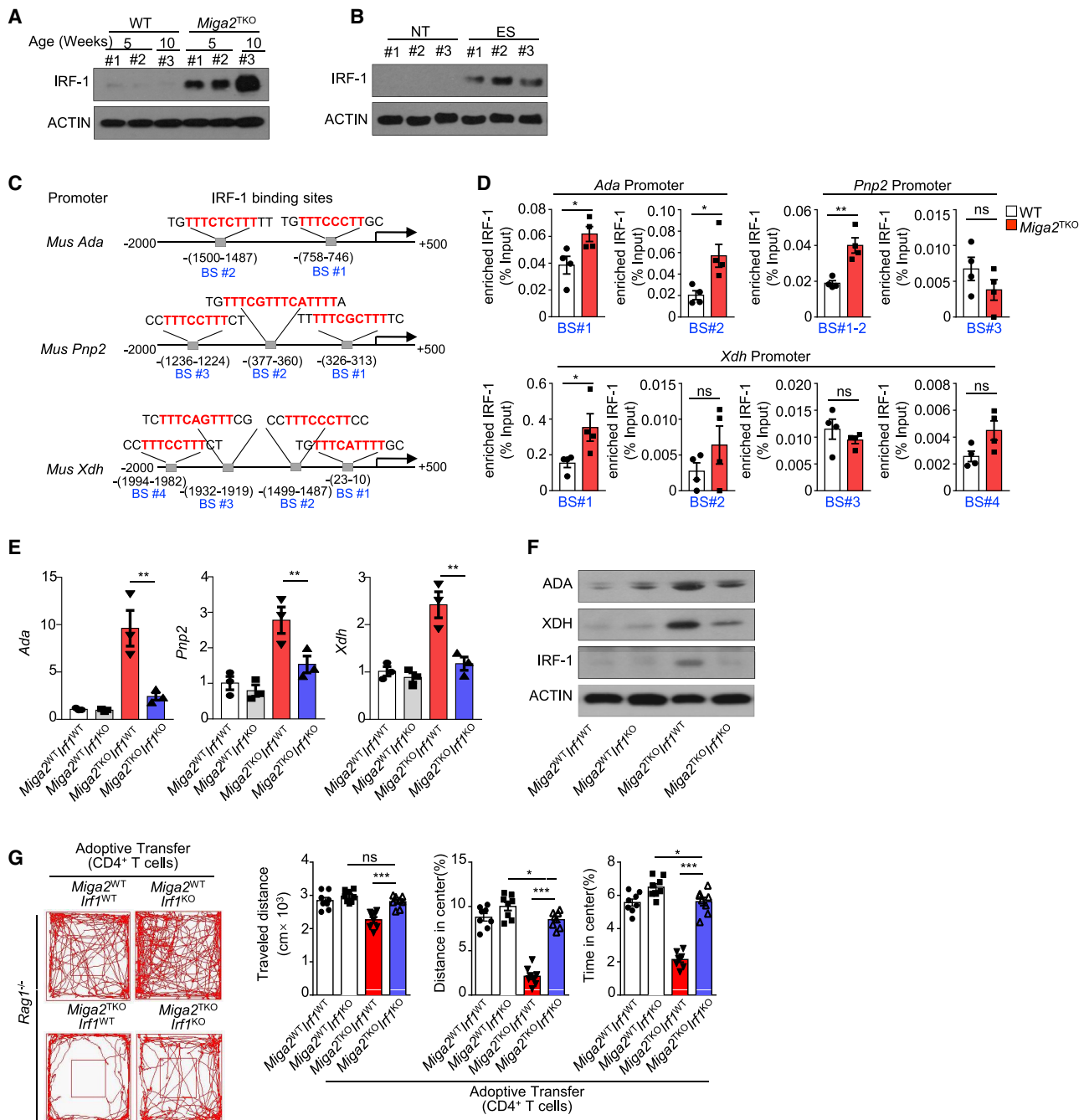


Figure 7. Accumulated IRF-1 Controls Purine Synthesis in CD4⁺ T Cells and Anxiety-like Behavior

- (A) IB analysis of IRF-1 expression in naive splenic CD4⁺ T cells from WT and *Miga2*^{TKO} mice.
- (B) The protein levels of IRF-1 in naive splenic CD4⁺ T cells from NT- and ES-treated mice was evaluated by IB.
- (C) Schematic representation of IRF1-binding sites (BS) in the promoters of the mouse *Ada*, *Xdh*, and *Pnp2* genes. BS, binding site. The sequences in red indicate IFN-stimulated responsive elements (ISREs).
- (D) ChIP-QPCR assays show the abundance of IRF-1 binding on these promoters. The results are presented relative to the total input DNA.
- (E-F) The mRNA and protein levels of indicated genes in *Miga2*^{TKO} *Irf1*^{-/-} naive CD4⁺ T cells were monitored by qRT-PCR (E) and IB (F).
- (G) *Rag1*^{-/-} mice were adoptively transferred with 5 × 10⁶ *Miga2*^{TKO} *Irf1*^{-/-} CD4⁺ T cells every other day. Six days later, the anxiety-like behavior of these recipient *Rag1*^{-/-} mice was evaluated by the OFT (n = 8).
- All data are representative of at least three independent experiments. Data are represented as means ± SEM. The significances of difference in (E) and (G) were determined by Dunnett's test, and others were determined by t test. ns, no significance; *p < 0.01; **p < 0.005.

STAR★METHODS

Detailed methods are provided in the online version of this paper and include the following:

- **KEY RESOURCES TABLE**
- **LEAD CONTACT AND MATERIALS AVAILABILITY**
- **EXPERIMENTAL MODEL AND SUBJECT DETAILS**
 - Mice
 - Patients and Samples preparation
 - Study approval
- **METHOD DETAILS**
 - Electric shock model
 - Restraint stress model
 - Open-field test
 - Elevated plus maze test
 - Tail suspension test
 - Light–Dark box test
 - T cell depletion and drug treatment
 - Induction and assessment of EAE
 - T cell purification and adoptive transfers
 - RNA-seq analysis
 - Fluorescence microscopy
 - T cell isolation and stimulation
 - Transmission Electron Microscopy
 - CD4⁺ T cell proliferation
 - Single cell dissociation
 - Flow cytometry and intracellular cytokine staining
 - Metabolic Assays
 - Isolation of oligodendrocytes
 - Viral injection
 - LC-MS analysis for serum metabolome
 - ¹³C tracing by liquid-chromatography Q-exactive mass spectrometry (LC-QEMS)
 - qRT-PCR
 - Immunoblot (IB)
 - Chromatin IP (ChIP) assay
 - Tissue staining/IHC
 - *In vivo* BrdU proliferation assay
- **QUANTIFICATION AND STATISTICAL ANALYSIS**
- **DATA AND CODE AVAILABILITY**

SUPPLEMENTAL INFORMATION

Supplemental Information can be found online at <https://doi.org/10.1016/j.cell.2019.10.001>.

ACKNOWLEDGMENTS

We thank Bangguo Qian from PerkinElmer for the technical support. We thank Dian Wang (Hangzhou Neoline Technology Co., Ltd.) for the technical support in using Tissue Gnostics TissueFAXS6.0.123. We thank Jia-shu Yao for the clinical sample collection. Thanks also go to the Life Sciences Institute core facilities, Zhejiang University for technical assistance. This study was supported by the National Key R&D Program of China (2018YFA0800503 and 2018YFD0500100), Excellent Young Scientist Fund of NSFC (31822017), Zhejiang Provincial Natural Science Foundation of China (LR19C080001), the Strategic Priority Research Program of the Chinese Academy of Science (XDA16010302), and the National Natural Science Foundation of China (81572651, 81771675, 81622013, and 81700913).

AUTHOR CONTRIBUTIONS

Conceptualization, J.J. and Y.-Y.L.; Methodology, K.F., Y.-Y.L., and H.W.; Software, X.-T.M. and Y.-N.L.; Formal Analysis, J.G. and L.S.; Investigation, K.F., Y.-Y.L., H.W., F.W., X.-Y.M., Z.G., Lei Zhang, and K.R.; Resources, L.H., W.C., D.Q., W.X., Q.C., Long Zhang, C.T., L.L., W.L., G.Z., Y.W., M.T., and R.C.; Data Curation, J.Z.; Writing – Original Draft, J.J., K.F., Y.-Y.L., and R.C.; Writing – Review & Editing, J.J. and X.F.; Visualization, J.J., K.F., Y.-Y.L., and H.W.; Supervision, J.J.; Funding Acquisition, J.J. and R.C.

DECLARATION OF INTERESTS

The authors declare no competing interests.

Received: April 15, 2019

Revised: August 15, 2019

Accepted: October 1, 2019

Published: October 31, 2019

REFERENCES

- Ali-Sisto, T., Tolmunen, T., Toffol, E., Viinämäki, H., Mäntyselkä, P., Valkonen-Korhonen, M., Honkalampi, K., Ruusunen, A., Velagapudi, V., and Lehto, S.M. (2016). Purine metabolism is dysregulated in patients with major depressive disorder. *Psychoneuroendocrinology* 70, 25–32.
- Arpaia, E., Benveniste, P., Di Cristofano, A., Gu, Y., Dalal, I., Kelly, S., Hershfeld, M., Pandolfi, P.P., Roifman, C.M., and Cohen, A. (2000). Mitochondrial basis for immune deficiency. Evidence from purine nucleoside phosphorylase-deficient mice. *J. Exp. Med.* 191, 2197–2208.
- Beurel, E., Harrington, L.E., and Jope, R.S. (2013). Inflammatory T helper 17 cells promote depression-like behavior in mice. *Biol. Psychiatry* 73, 622–630.
- Bourin, M., Petit-Demoulière, B., Dhonchadha, B.N., and Hascöt, M. (2007). Animal models of anxiety in mice. *Fundam. Clin. Pharmacol.* 21, 567–574.
- Brachman, R.A., Lehmann, M.L., Maric, D., and Herkenham, M. (2015). Lymphocytes from chronically stressed mice confer antidepressant-like effects to naïve mice. *J. Neurosci.* 35, 1530–1538.
- Buck, M.D., O'Sullivan, D., Klein Geltink, R.I., Curtis, J.D., Chang, C.H., Sanin, D.E., Qiu, J., Kretz, O., Braas, D., van der Windt, G.J., et al. (2016). Mitochondrial Dynamics Controls T Cell Fate through Metabolic Programming. *Cell* 166, 63–76.
- Campos, A.C., Fogaça, M.V., Aguiar, D.C., and Guimarães, F.S. (2013). Animal models of anxiety disorders and stress. *Br. J. Psychiatry* 35 (Suppl 2), S101–S111.
- Chourbaji, S., Urani, A., Inta, I., Sanchis-Segura, C., Brandwein, C., Zink, M., Schwaninger, M., and Gass, P. (2006). IL-6 knockout mice exhibit resistance to stress-induced development of depression-like behaviors. *Neurobiol. Dis.* 23, 587–594.
- Clark, S.M., Sand, J., Francis, T.C., Nagaraju, A., Michael, K.C., Keegan, A.D., Kusnecov, A., Gould, T.D., and Tonelli, L.H. (2014). Immune status influences fear and anxiety responses in mice after acute stress exposure. *Brain Behav. Immun.* 38, 192–201.
- Clark, S.M., Michael, K.C., Klaus, J., Mert, A., Romano-Verthelyi, A., Sand, J., and Tonelli, L.H. (2015). Dissociation between sickness behavior and emotionality during lipopolysaccharide challenge in lymphocyte deficient Rag2(-/-) mice. *Behav. Brain Res.* 278, 74–82.
- Cushman, J., Lo, J., Huang, Z., Wasserfall, C., and Petitto, J.M. (2003). Neurobehavioral changes resulting from recombinase activation gene 1 deletion. *Clin. Diagn. Lab. Immunol.* 10, 13–18.
- Darashchonak, N., Koepsell, B., Bogdanova, N., and von Versen-Höynck, F. (2014). Adenosine A2B receptors induce proliferation, invasion and activation of cAMP response element binding protein (CREB) in trophoblast cells. *BMC Pregnancy Childbirth* 14, 2.
- Davis, M. (1992). The role of the amygdala in fear and anxiety. *Annu. Rev. Neurosci.* 15, 353–375.

- de Kloet, E.R., Joëls, M., and Holsboer, F. (2005). Stress and the brain: from adaptation to disease. *Nat. Rev. Neurosci.* 6, 463–475.
- Dhabhar, F.S. (2008). Enhancing versus Suppressive Effects of Stress on Immune Function: Implications for Immunoprotection versus Immunopathology. *Allergy Asthma Clin. Immunol.* 4, 2–11.
- Dimsdale, J.E. (2008). Psychological stress and cardiovascular disease. *J. Am. Coll. Cardiol.* 51, 1237–1246.
- Dragoş, D., and Tănasescu, M.D. (2010). The effect of stress on the defense systems. *J. Med. Life* 3, 10–18.
- Engelhardt, B., Vajkoczy, P., and Weller, R.O. (2017). The movers and shapers in immune privilege of the CNS. *Nat. Immunol.* 18, 123–131.
- Engler, H., Brendt, P., Wischermann, J., Wegner, A., Röhling, R., Schoemberg, T., Meyer, U., Gold, R., Peters, J., Benson, S., and Schedlowski, M. (2017). Selective increase of cerebrospinal fluid IL-6 during experimental systemic inflammation in humans: association with depressive symptoms. *Mol. Psychiatry* 22, 1448–1454.
- Filiano, A.J., Xu, Y., Tustison, N.J., Marsh, R.L., Baker, W., Smirnov, I., Overall, C.C., Gadani, S.P., Turner, S.D., Weng, Z., et al. (2016). Unexpected role of interferon- γ in regulating neuronal connectivity and social behaviour. *Nature* 535, 425–429.
- Gao, Z., Li, Y., Wang, F., Huang, T., Fan, K., Zhang, Y., Zhong, J., Cao, Q., Chao, T., Jia, J., et al. (2017). Mitochondrial dynamics controls anti-tumour innate immunity by regulating CHIP-IRF1 axis stability. *Nat. Commun.* 8, 1805.
- Glaser, R., and Kiecolt-Glaser, J.K. (2005). Stress-induced immune dysfunction: implications for health. *Nat. Rev. Immunol.* 5, 243–251.
- Gracie, D.J., and Ford, A.C. (2019). Depression, Antidepressants, and Inflammatory Bowel Disease: Implications for Future Models of Care. *Gastroenterology* 156, 2345–2347.
- Kipnis, J. (2016). Multifaceted interactions between adaptive immunity and the central nervous system. *Science* 353, 766–771.
- Krishnan, V., and Nestler, E.J. (2008). The molecular neurobiology of depression. *Nature* 455, 894–902.
- Langlais, D., Barreiro, L.B., and Gros, P. (2016). The macrophage IRF8/IRF1 regulome is required for protection against infections and is associated with chronic inflammation. *J. Exp. Med.* 213, 585–603.
- Lécuyer, M.-A., Saint-Laurent, O., Bourbonnière, L., Larouche, S., Larochelle, C., Michel, L., Charabati, M., Abadier, M., Zandee, S., Haghayegh Jahromi, N., et al. (2017). Dual role of ALCAM in neuroinflammation and blood-brain barrier homeostasis. *Proc. Natl. Acad. Sci. USA* 114, E524–E533.
- Lewitus, G.M., Wilf-Yarkoni, A., Ziv, Y., Shabat-Simon, M., Gersner, R., Zangen, A., and Schwartz, M. (2009). Vaccination as a novel approach for treating depressive behavior. *Biol. Psychiatry* 65, 283–288.
- Li, C.M., Tyler, P.C., Furneaux, R.H., Kicska, G., Xu, Y., Grubmeyer, C., Girvin, M.E., and Schramm, V.L. (1999). Transition-state analogs as inhibitors of human and malarial hypoxanthine-guanine phosphoribosyltransferases. *Nat. Struct. Biol.* 6, 582–587.
- Li, Z., Ma, L., Kulesskaya, N., Völkar, V., and Tian, L. (2014). Microglia are polarized to M1 type in high-anxiety inbred mice in response to lipopolysaccharide challenge. *Brain Behav. Immun.* 38, 237–248.
- Li, Y., Singer, N.G., Whitbred, J., Bowen, M.A., Fox, D.A., and Lin, F. (2017). CD6 as a potential target for treating multiple sclerosis. *Proc. Natl. Acad. Sci. USA* 114, 2687–2692.
- Markert, M.L. (1991). Purine nucleoside phosphorylase deficiency. *Immuno-defic. Rev.* 3, 45–81.
- McEwen, B.S., Bowles, N.P., Gray, J.D., Hill, M.N., Hunter, R.G., Karatsoreos, I.N., and Nasca, C. (2015). Mechanisms of stress in the brain. *Nat. Neurosci.* 18, 1353–1363.
- McKim, D.B., Weber, M.D., Niraula, A., Sawicki, C.M., Liu, X., Jarrett, B.L., Ramirez-Chan, K., Wang, Y., Roeth, R.M., Sucaldito, A.D., et al. (2018). Microglial recruitment of IL-1 β -producing monocytes to brain endothelium causes stress-induced anxiety. *Mol. Psychiatry* 23, 1421–1431.
- Miles, R.W., Tyler, P.C., Furneaux, R.H., Bagdassarian, C.K., and Schramm, V.L. (1998). One-third-the-sites transition-state inhibitors for purine nucleoside phosphorylase. *Biochemistry* 37, 8615–8621.
- Mishra, P., and Chan, D.C. (2016). Metabolic regulation of mitochondrial dynamics. *J. Cell Biol.* 212, 379–387.
- Miyajima, M., Zhang, B., Sugiura, Y., Sonomura, K., Guerrini, M.M., Tsutsui, Y., Maruya, M., Vogelzang, A., Chamoto, K., Honda, K., et al. (2017). Metabolic shift induced by systemic activation of T cells in PD-1-deficient mice perturbs brain monoamines and emotional behavior. *Nat. Immunol.* 18, 1342–1352.
- Naidoo, J., Page, D.B., Li, B.T., Connell, L.C., Schindler, K., Lacouture, M.E., Postow, M.A., and Wolchok, J.D. (2015). Toxicities of the anti-PD-1 and anti-PD-L1 immune checkpoint antibodies. *Ann. Oncol.* 26, 2375–2391.
- Padgett, D.A., and Glaser, R. (2003). How stress influences the immune response. *Trends Immunol.* 24, 444–448.
- Phelps, E.A., O'Connor, K.J., Gatenby, J.C., Gore, J.C., Grillon, C., and Davis, M. (2001). Activation of the left amygdala to a cognitive representation of fear. *Nat. Neurosci.* 4, 437–441.
- Phillis, J.W., and Wu, P.H. (1982). Adenosine mediates sedative action of various centrally active drugs. *Med. Hypotheses* 9, 361–367.
- Ransohoff, R.M., and Engelhardt, B. (2012). The anatomical and cellular basis of immune surveillance in the central nervous system. *Nat. Rev. Immunol.* 12, 623–635.
- Rattazzi, L., Piras, G., Ono, M., Deacon, R., Pariante, C.M., and D'Acquisto, F. (2013). CD4 $^{+}$ but not CD8 $^{+}$ T cells revert the impaired emotional behavior of immunocompromised RAG-1-deficient mice. *Transl. Psychiatry* 3, e280.
- Reiche, E.M.V., Nunes, S.O.V., and Morimoto, H.K. (2004). Stress, depression, the immune system, and cancer. *Lancet Oncol.* 5, 617–625.
- Rilett, K.C., Friedel, M., Ellegood, J., MacKenzie, R.N., Lerch, J.P., and Foster, J.A. (2015). Loss of T cells influences sex differences in behavior and brain structure. *Brain Behav. Immun.* 46, 249–260.
- Shackman, A.J., and Fox, A.S. (2016). Contributions of the Central Extended Amygdala to Fear and Anxiety. *J. Neurosci.* 36, 8050–8063.
- Steimer, T. (2011). Animal models of anxiety disorders in rats and mice: some conceptual issues. *Dialogues Clin. Neurosci.* 13, 495–506.
- Stoop, J.W., Zegers, B.J.M., Hendrickx, G.F.M., van Heukelom, L.H., Staal, G.E.J., de Bree, P.K., Wadman, S.K., and Ballieux, R.E. (1977). Purine nucleoside phosphorylase deficiency associated with selective cellular immunodeficiency. *N. Engl. J. Med.* 296, 651–655.
- Tamashiro, K.L., Sakai, R.R., Shively, C.A., Karatsoreos, I.N., and Reagan, L.P. (2011). Chronic stress, metabolism, and metabolic syndrome. *Stress* 14, 468–474.
- Theien, B.E., Vanderlugt, C.L., Eagar, T.N., Nickerson-Nutter, C., Nazareno, R., Kuchroo, V.K., and Miller, S.D. (2001). Discordant effects of anti-VLA-4 treatment before and after onset of relapsing experimental autoimmune encephalomyelitis. *J. Clin. Invest.* 107, 995–1006.
- Thomas, K.M., Drevets, W.C., Dahl, R.E., Ryan, N.D., Birmaher, B., Eccard, C.H., Axelson, D., Whalen, P.J., and Casey, B.J. (2001). Amygdala response to fearful faces in anxious and depressed children. *Arch. Gen. Psychiatry* 58, 1057–1063.
- Uhlik, M., Good, L., Xiao, G., Harhaj, E.W., Zandi, E., Karin, M., and Sun, S.-C. (1998). NF- κ B-inducing kinase and IkB kinase participate in human T-cell leukemia virus I Tax-mediated NF- κ B activation. *J. Biol. Chem.* 273, 21132–21136.
- Vajkoczy, P., Laschinger, M., and Engelhardt, B. (2001). α 4-integrin-VCAM-1 binding mediates G protein-independent capture of encephalitogenic T cell blasts to CNS white matter microvessels. *J. Clin. Invest.* 108, 557–565.
- Wai, T., and Langer, T. (2016). Mitochondrial Dynamics and Metabolic Regulation. *Trends Endocrinol. Metab.* 27, 105–117.
- Wakabayashi, C., Numakawa, T., Odaka, H., Ooshima, Y., Kiyama, Y., Manabe, T., Kunugi, H., and Iwakura, Y. (2015). IL-1 receptor-antagonist (IL-1Ra) knockout mice show anxiety-like behavior by aging. *Neurosci. Lett.* 599, 20–25.

- Wang, Y.-L., Han, Q.-Q., Gong, W.-Q., Pan, D.-H., Wang, L.-Z., Hu, W., Yang, M., Li, B., Yu, J., and Liu, Q. (2018). Microglial activation mediates chronic mild stress-induced depressive- and anxiety-like behavior in adult rats. *J. Neuroinflammation* 15, 21.
- Wohleb, E.S., Hanke, M.L., Corona, A.W., Powell, N.D., Stiner, L.M., Bailey, M.T., Nelson, R.J., Godbout, J.P., and Sheridan, J.F. (2011). β -Adrenergic receptor antagonism prevents anxiety-like behavior and microglial reactivity induced by repeated social defeat. *J. Neurosci.* 31, 6277–6288.
- Zhan, M., Brooks, C., Liu, F., Sun, L., and Dong, Z. (2013). Mitochondrial dynamics: regulatory mechanisms and emerging role in renal pathophysiology. *Kidney Int.* 83, 568–581.

STAR★METHODS

KEY RESOURCES TABLE

REAGENT or RESOURCE	SOURCE	IDENTIFIER
Antibodies		
Rabbit monoclonal anti-Adenosine A1 Receptor(clone EPR6179), Alexa Fluor 488	Abcam	Cat# ab202949
Rabbit monoclonal anti-Myelin oligodendrocyte glycoprotein(clone EP4281), Alexa Fluor 647	Abcam	Cat# ab199472
Rabbit monoclonal anti-NeuN(clone EPR12763), Alexa Fluor 568	Abcam	Cat# ab207282
Rabbit polyclonal anti-c-Fos(clone 2H2)	Abcam	Cat# ab208942; RRID: AB_2747772
Rabbit polyclonal anti-Adenosine A2a Receptor	Abcam	Cat# ab3461; RRID: AB_303823
Rabbit polyclonal anti-Adenosine A2b Receptor	Abcam	Cat# ab222901
Rabbit polyclonal anti-Adenosine A3 Receptor	Abcam	Cat# ab203298
Rabbit monoclonal anti-IRF1(clone EPR18301)	Abcam	Cat# ab186384
Mouse monoclonal anti-Mitofusin 2(clone 6A8)	Abcam	Cat# ab56889; RRID: AB_2142629
Rabbit polyclonal anti-ADA	Abcam	Cat# ab175310
Rabbit monoclonal anti- Xanthine Oxidase [EPR4605]	Abcam	Cat# ab109235; RRID: AB_10863199
Mouse monoclonal anti-GFAP(clone 2E1.E9), Brilliant Violet 421	Biolegend	Cat# 644710; RRID: AB_2566685
Mouse monoclonal anti-CX3CR1(clone SA011F11), PE	Biolegend	Cat# 149015; RRID: AB_2565699
Mouse monoclonal anti-IRF1(clone E-4)	Santa Cruz	Cat# sc-514544
Anti-BrdU(clone 3D4), Alexa Fluor 488	BD	Cat# 558599; RRID: AB_647075
Mouse monoclonal anti-β-Actin(clone AC-74)	Sigma	Cat# A2228; RRID: AB_476697
Rat Anti-mouse B220(clone RA3-6B2), PE	BD	Cat# 553089; RRID: AB_394619
Hamster monoclonal anti-CD3e (clone 145-2C11), APC	eBioscience	Cat# 17-0031-83; RRID: AB_469316
Rat monoclonal anti-CD4(clone RM4-5), eFluor 450	eBioscience	Cat# 48-0042-82; RRID: AB_1272194
Rat monoclonal anti-CD8a(clone 53-6.7), PerCP-Cyanine5.5	eBioscience	Cat# 45-0081-82; RRID: AB_1107004
Rat anti-mouse CD44(clone IM7), FITC	BD	Cat# 561859; RRID: AB_10894581
Rat monoclonal anti-CD62L(clone MEL-14), APC	eBioscience	Cat# 17-0621-83; RRID: AB_469411
Anti-mouse CD4(clone GK 1.5)	BioXcell	Cat# BE0003-1; RRID: AB_1107636
Anti-mouse/human CD49d(clone PS/2)	BioXcell	Cat# BE0071; RRID: AB_1107657
Anti-mouse CD8a(clone 2.43)	BioXcell	Cat# BE0061; RRID: AB_1125541
Anti-O4 MicroBeads	Mitenyi	Cat# 130-094-543
Anti-CD4 MicroBeads	Mitenyi	Cat# 130-117-043
Phospho-PKA Substrate (RRXS*/T*) (100G7E)	Cell Signaling technology	Cat# 9624; RRID: AB_331817
Bacterial and Virus Strains		
AAV9-GFAP-GFP-miR30-shRNA(mAdora1)	vigenebio	N/A
AAV8-MBP-GFP-miR30-shRNA(mAdora1)	vigenebio	N/A
AAV8-MBP-GFP-miR30-shRNA(scramble)	vigenebio	N/A

(Continued on next page)

Continued

REAGENT or RESOURCE	SOURCE	IDENTIFIER
Biological Samples		
Patient's and healthy people's serum	Sir Run Run Shaw Hospital	http://www.srrsh-english.com
Patient's and healthy people's serum	Nanjing Drum Tower Hospital	http://www.njglyy.com
Chemicals, Peptides, and Recombinant Proteins		
Deoxycholic acid	yuanye bio	Cat# S24458
vidarabine	yuanye bio	Cat# S18122
Adenine	yuanye bio	Cat# S18009
2-DG	yuanye bio	Cat# S11070
Sodium taurochenodeoxycholate	yuanye bio	Cat# S31336
Prostaglandin B1	yuanye bio	Cat# ZC-20354
leukotriene B4	yuanye bio	Cat# ZC-22879
15-deoxy-D12,14-prostaglandin J2	yuanye bio	Cat# ZC-22860
γ-GABA	yuanye bio	Cat# S20180
DL-adrenaline	yuanye bio	Cat# S64536
Dicortol	yuanye bio	Cat# S31439
BCX-1777	MCE	Cat# HY-16209
BLZ945	Topscience	Cat# T6119
pexidartinib	Topscience	Cat# T2115
xanthine	aladdin	Cat# H108384
hypoxanthine	aladdin	Cat# X104264
papain	sigma	Cat# P4762
7-AAD (7-amino-actinomycin D)	BD	Cat# 559925
BrdU	Sangon	Cat# E607203
DAPI	Biolegend	Cat# 422801
Mitospy orange CMTMRos	Biolegend	Cat# 424803
D-Glucose- ¹³ C ₆	sigma	Cat# 389374
Critical Commercial Assays		
Mouse xanthine ELISA kit	Sangon	Cat# D720328
FITC Annexin V Apoptosis Detection Kit I	BD	Cat# 556547
Lightning-Link Kit(FITC)	Innova Biosciences	707-0010
Lightning-Link Kit(APC)	Innova Biosciences	705-0010
Lightning-Link Kit(PE)	Innova Biosciences	703-0010
Lightning-Link Kit(Percp5.5)	Innova Biosciences	763-0030
Deposited Data		
Raw and analyzed data	This paper	PRJNA528163
Experimental Models: Organisms/Strains		
Mouse: C57BL/6J	The Jackson Laboratory	CAT#000664
Mouse: B6.129S7- <i>Rag1</i> ^{tm1Mmom} /J	The Jackson Laboratory	CAT#02216
B6.Cg-Tg(Cd4-cre) ^{1Cwi/BfluJ}	The Jackson Laboratory	CAT#022071
Mouse: B6- <i>Fam73btm1a(KOMP)Wtsi</i> (<i>Miga2</i> ^{-/-})	University of California, Davis Knockout Mouse Project Repository	CAT#048607-UCD
Mouse: B6.129S2- <i>Irf1</i> ^{tm1Mak} /J	The Jackson Laboratory	CAT#002762
Mouse: B6- <i>Pnp2</i> -eKO1	Shanghai Model Organisms Center, Inc	https://www.modelorg.com
Mouse: B6- <i>Mfn1</i> ^{flox} - <i>Mfn2</i> ^{flox}	Dr. Yuan Wang (East China Normal University)	N/A
Oligonucleotides		
Primers for genotyping, see Table S7	This paper	N/A
Primers for qPRC, see Table S8	This paper	N/A
Primers for CHIP-qPRC, see Table S8	This paper	N/A

(Continued on next page)

Continued

REAGENT or RESOURCE	SOURCE	IDENTIFIER
Software and Algorithms		
TissueFAXS6.0.123	Neoline	N/A
ImageJ		https://imagej.nih.gov/ij/
10x Cell Ranger package	10x Genomics	https://support.10xgenomics.com
FlowJo	Treestar	https://www.flowjo.com
Prism	GraphPad	https://www.graphpad.com
Other		
4-0 silk	Ethicon	Cat# W501
6-0 silk	Ethicon	Cat# W580
hemostat	Scanlan	Cat# 4635-06
needle holder	Scanlan	Cat# 6006-05

LEAD CONTACT AND MATERIALS AVAILABILITY

Further information and requests for reagents should be directed to and will be fulfilled by the Lead Contact, Jin Jin (jjin4@zju.edu.cn).

All materials generated in this study are available for requests.

EXPERIMENTAL MODEL AND SUBJECT DETAILS**Mice**

Miga2 KOfirst mice (C57BL/6 background) were a gift from the Prof. Heng-Yu Fan (Zhejiang University, P. R. China). *Miga2* KOfirst mice were targeted exon 3 of *Miga2* gene using a FRT-LoxP vector. *Miga2*-floxed mice were generated by crossing the *Miga2* KOfirst mice with FLP deleter mice (Rosa26-FLPe; Jackson Laboratory). The *Miga2*-floxed mice were further crossed with *Cd4*-Cre mice (all from Jackson Laboratory, C57BL/6 background) to generate T cell conditional *Miga2* KO (*Miga2*^{f/f}*Cd4*-Cre, TKO) mice. *Irf1*^{−/−} mice (C57BL/6 background) were provided by Prof. Shu-yu Zhang (Sichuan University, China). *Mfn1*^{fl/fl}*Mfn2*^{fl/fl} mice (C57BL/6 background) were provided by Prof. Yuan Wang (East China University of Science and Technology, China), and further crossed with *Cd4*-Cre mice to generate *Mfn1*-*Mfn2* T cell conditional double KO mice. *Pnp2*^{−/−} mice in B6 background was generated by Shanghai Model Organisms Center, Inc (SMOC) by targeting of exon 2 of *Pnp2* using CRISPR/CAS9.

Heterozygous mice were bred to generate littermate controls and KO (or conditional KO) mice for experiments. In the animal studies, WT and multiple KO mice at the age of 6–8 weeks are randomly grouped. Outcomes of animal experiments were collected blindly and recorded based on ear-tag numbers of the experimental mice. The different sex did not affect the final conclusion, thus male and female mice were equally grouped in the behavior test. The Genotyping primers were performed in Table S7. Mice were maintained in specific pathogen-free (SPF) facility with room temperature, and all animal experiments were conducted in accordance with protocols approved by the Institutional Animal Care and Use Committee of Zhejiang University.

Patients and Samples preparation

Sample collection was performed at Sir Runrun Shaw Hospital and Nanjing Drum Tower Hospital between January and August 2019. Informed written consent was obtained from all participants. The Inclusion criteria were: 20 males and 20 females; age between 18 and 65 years; diagnosed with anxiety disorders according to the ICD-10 criteria; assess mood and anxiety symptoms through the Hamilton Anxiety Scale. The exclusion criteria were: using drugs targeting purine metabolism; complication with other autoimmune diseases; severe brain injuries or brain lesions have occurred. The inclusion criteria of control subjects were: age between 18 and 65 years; no psychiatric disorders according to ICD-10 criteria; no serious systemic diseases; no complications and tumor. Control group also matched the above exclusion criteria.

All blood samples of patients and healthy individuals were collected at 6:00 am, followed by centrifugation (3000 g, 10 min) to remove cells and debris, and then the serums were stored at −80°C until further analysis.

Study approval

All animal experiments were conducted in accordance with protocols (#12077) approved by the Institutional Animal Care and Use Committee of Zhejiang University.

For human studies, written informed consents were obtained from all subjects before the study protocol. All human experiments were conducted in accordance with protocols (#20190319-4) approved by the Medical Ethics Committee of Sir Run Run Shaw Hospital, Zhejiang University and Nanjing Drum Tower Hospital.

METHOD DETAILS

Electric shock model

All animals were allowed to the experimental room for 1 h before the training. Mice were individually placed in a chamber with a grid floor connected to a shock generator. Two min after being placed in the chamber, the mice were exposed to a 3 s foot shock (0.6 mA) for 5 times during 120 s randomly for 8 or 30 consecutive days. For the control group, mice were placed in the chamber at the same time without foot shock. After training, mice were placed back into their home cages. Training chambers were cleaned with 75% ethanol before and after each trial to avoid any olfactory cues.

Restraint stress model

Mice were subjected to RS by placement in a small cage (5cm × 5cm × 5cm) and subjected for 6 h restraint from 9:00 a.m. to 3:00 p.m. during 8 or 30 consecutive days. The holes along the sidewall of the cages enabled air flowing. Animals could move head and the body but were not able to jump or run. The mice had no access to food and water during the restraint. Once the restraint ended, mice were put back to their home cages immediately with access to food and water freely. For the control group, the mice were placed in the home cage at the same time without food and water.

Open-field test

Mice were gently placed in the center of a white plastic open-field arena (50cm × 50cm × 50cm) and allowed to explore freely for 5 min. A video camera positioned directly above the arena was used to track the movement of each animal, and recorded on a computer with software (Any-maze by Stoelting) to track the total distance and the amount of time spent in the center of the chamber compared to the edges. Open field test is commonly used for measuring the exploratory behavior and general activity of animals. The test room were dark and sound-insulated, tracking instrument recognized mouse central body point with infrared lasers and sensors.

More time spent in the edges of the box with less time spent in the center of the box is interpreted as anxiety-like behavior. Before the test, the mice were acclimatized to the room for 1 h, and the arena was cleaned with 70% EtOH after every trial.

Elevated plus maze test

Mice were introduced into the center quadrant of a 4-arm maze with two open arms without walls and two closed arms with walls (25cm long, 5cm wide). This structure was elevated 60 cm above the floor. The mice were placed in the center and faced to a closed arm at the start of a trial. A video camera positioned directly above the arena was used to track the movement of each animal, and recorded on a computer with software (Any-maze by Stoelting). This software tracked the amount of time the mice spent in the closed arms versus the open arms throughout a 5-min session. Higher anxiety is indicated by a lower frequency of movement into open arms and less time spent there. Before the test, mice were acclimatized to the room for 1 h, and the arena was cleaned with 70% EtOH after every trial.

Tail suspension test

Mice were suspended by their tails with tape in a position that they could not escape or hold on to nearby surfaces for 6 min. This test is based on the fact that animals subjected to a short-term inescapable stress will develop an immobile posture. The total duration of the test can be divided into periods of agitation and immobility. Video tracking data were analyzed using software to extract the resulting escape-oriented behaviors. Higher depression is indicated by less time spent trying to escape.

Light-Dark box test

Mice were gently placed in a cage (50 × 25 × 25cm) divided into a small dark compartment (one-third) and a large illuminated compartment (two-thirds) by a partition with a door. The mice were allowed to move freely between the two chambers with the door open for 5 min. Video tracking data was analyzed using software to extract the movement trail and the time spent in each compartment. Based on the innate aversion of rodents to brightly illuminated areas and spontaneous exploratory behavior of the mice, the time spent in the dark chamber could serve as an index of anxiety-like behavior.

T cell depletion and drug treatment

For the depletion of CD4⁺ or CD8⁺ T cells, mice were injected intravenously (i.v.) with 500 µg anti-CD4 antibody (GK 1.5) or 500 µg anti-CD8 antibody (2.43) every 7 days. To inhibit leukocyte migration into the brain, mice were injected intravenously (i.v.) with anti-VLA-4 (α VLA-4, 20 mg/kg) or anti-CD6 (α CD6, 10 mg/kg) every three days. All antibodies were stocked in fridge and diluted to their working concentrations in PBS. Mice in control group were injected with PBS of the same volume at same time intraperitoneally.

For drug treatment experiment, the solutions of drugs (2-DG/adenine/xanthine/pnp2 inhibitor) were prepared freshly each time with 0.9% saline. 8-weeks-old mice were intraperitoneally injected with drug solution depending on their working doses on day 0, day 3 and day 6. The treatment continued one week until Open-field behavior testing was performed on day 8. For control group, mice were intraperitoneally injected with 0.9% saline of the same volume at same time.

Induction and assessment of EAE

For active EAE induction, age- and sex-matched mice were immunized s.c. with MOG₃₅₋₅₅ peptide (300 µg) mixed in CFA (Sigma-Aldrich) containing 5 mg/mL heat-killed *Mycobacterium tuberculosis* H37Ra (Difco). Pertussis toxin (200 ng, List Biological Laboratories) in PBS was administered i.v. on days 0 and 2. Mice were examined daily and scored for disease severity using the standard scale: 0, no clinical signs; 1, limp tail; 2, paraparesis (weakness, incomplete paralysis of one or two hind limbs); 3, paraplegia (complete paralysis of two hind limbs); 4, paraplegia with forelimb weakness or paralysis; 5, moribund or death. After the onset of EAE, food and water were provided on the cage floor. Mononuclear cells were prepared from the CNS (brain and spinal cord) of EAE-induced mice and analyzed by flow cytometry.

T cell purification and adoptive transfers

CD4⁺ T cells were purified by positive magnetic cell sorting (CD4⁺ T cell isolation kit, Miltenyi Biotec) from the spleens and lymph nodes of 6-8 weeks-old mice. For some experiments, purified CD4⁺ T cells were further sorted on a FACS AriaII cell sorter (BD Biosciences) to obtain naive CD4⁺ T cells (CD4⁺CD44^{lo}CD62L^{hi}) using anti-CD44-FITC and anti-CD62L-APC antibodies. Sorted cells were spin down and washed with PBS and prepared for the following experiments.

For adoptive transfer experiments, 5×10^6 purified CD4⁺ T cells, CD8⁺ T cells, 3×10^6 naive CD4⁺ T cells or 1.5×10^6 effector CD4⁺ T cells (CD4⁺CD44^{hi}CD62L^{lo}) were transferred by intravenous (i.v.) injection into mice grouped as indicated at day 0, 3 and 6. Control group were injected with PBS in the same time. Open-field behavior testing was taken at day 8.

RNA-seq analysis

Fresh splenic naive T cells were isolated from young WT, *Miga2*^{TKO} or *Miga2*^{-/-} mice (6–8 weeks-old). In some experiment, Fresh splenic CD4⁺ or CD8⁺ T cells were isolated from WT, RS or ES mice. These T cells were used for total RNA isolation with Trizol (Invitrogen), and subjected to RNA-seq analysis. RNA sequencing was performed by the Life Science Institute Sequencing and Microarray Facility using an Illumina sequencer. The raw reads were aligned to the mm10 reference genome (build mm10), using Tophat2 RNA-Seq alignment software. The mapping rate was 70% overall across all the samples in the dataset. HTseq-Count was used to quantify the gene expression counts from Tophat2 alignment files. Differential expression analysis was performed on the count data using R package DESeq2. P values obtained from multiple binomial tests were adjusted using FDR (BH). Significant genes are defined by a BH corrected p value of cut-off of 0.05 and fold-change of at least two.

Fluorescence microscopy

Naive CD4⁺ T cells (CD44^{lo}CD62L^{hi}, 5×10^5) were isolated and spread to 12-well plate containing 70% alcohol-pretreated slide for starvation 2 h. These CD4⁺ T cells were stained with 250 nM of MitoSpy™ Orange CMTMRos for 20 min, and fixed with 4% paraformaldehyde (PFA) for 20 min. Then the cells were washed with PBS for three times and stained with 10 µg/mL DAPI. All the samples were imaged on a confocal microscope LSM710 (Carl Zeiss) outfitted with a Plan-Apochromat 63x oil immersion objective lenses (Carl Zeiss). Data were collected using Carl Zeiss software ZEN 2010. For quantification of mitochondrial morphology in MitoSpyTM Orange CMTMRos-stained macrophages, scoring was analyzed with Image-Pro blindly. Short were cells with a majority of mitochondria less than 7 µm; long were cells in which the majority of mitochondria were more than 7 µm.

T cell isolation and stimulation

Primary CD4⁺ T cells were isolated from the spleen and lympho-nodes (LNs) of young adult mice (6–8 weeks old) using anti-CD4 magnetic beads (Miltenyi Biotec). Naive CD4⁺ cells were further purified by flow cytometric cell sorting based on CD4⁺CD44^{lo}CD62L^{hi} surface markers, respectively (Aria II). The cells were stimulated with plate-bound anti-CD3 (1 µg/mL) and anti-CD28 (1 µg/mL) in replicate wells of 96-well plates (0.2 million cells per well) for T cell proliferation and apoptosis, 48-well plates (0.4 million cells per well) for T cell differentiation, 12-well plates (10^6 cells per well) for quantitative RT-PCR (qRT-PCR). Where indicated, the cells were acutely stimulated using an antibody cross-linking protocol.

Transmission Electron Microscopy

WT and *Miga2* KO naive CD4⁺ T cells were washed in PBS and fixed in 2.5% GA on ice for 15 min. Then the cells were scrapped and put into a 1.5 mL EP tube. The GA solution was refreshed and the cells were suspending and incubated at 4°C overnight. Then, the cells were embedded into agarose gel. The gel was cut into small pieces, washed in PBS and post-fixed in 1% Osmic acid for 1-2 h. Then the samples were washed in PBS and dehydrated in a series of gradient ethanol (50%, 75%, 85%, 95% and 100% ethanol), each for 15 min. Then the samples were embedded in Epon resin. Embedded samples were cut into 60 nm ultrathin sections. Sections were counterstained with uranyl acetate and lead citrate. All the samples were observed using a Hitachi HT7700 electron microscope.

CD4⁺ T cell proliferation

Naive CD4⁺ T cells were isolated from spleens and LNs of WT or *Miga2*^{TKO} mice. For CFSE dilution assay, T cells were labeled in 5 µM CFSE (Life Technologies) in 37°C and washed with PBS for 3 times. The cells were normalized and cultured in 96-well plates with plate-coated anti-CD3 (1 µg/mL) and anti-CD28 (1 µg/mL) for 48 and 72 h. Sorted T cells were analyzed by flow-cytometry using CytoFlex (Beckman Coulter).

Single cell dissociation

Artificial cerebrospinal fluid was prepared as following: αCSF, in mM: 87 NaCl, 2.5 KCl, 1.25 NaH2PO4, 26 NaHCO3, 75 sucrose, 20 glucose, 1 CaCl₂, 7 MgSO₄, adjusted to pH 7.4, equilibrated in 95% O₂ and 5% CO₂. Mice were deeply anesthetized and perfused through the heart with cold αCSF prepared previously. The amygdala was collected after the brains were removed from the skull, and dissociated using Papain diluted in αCSF followed by manual trituration using pipettes. After 30 min enzymatic digestion at 37°C with shaking of the tube every 10 min, the suspensions were filtered through a αCSF-equilibrated 35 µm cell strainer. After filtering, the suspension was diluted in a large volume (50 mL total) ice-cold αCSF, followed by centrifugation (200 g, 5 min) to reduce debris. The supernatant was removed carefully and precipitated cells were resuspended in a minimal volume ice-cold DMEM containing 1% BSA. These suspensions were then carried out with 10x Genomics Chromium Single Cell Kit for Single-Cell RNA-seq. Importantly, αCSF equilibrated in 95% O₂ 5% CO₂ was used in all steps for improved cell viability, and cells were kept on ice or at 4°C at all times except for enzymatic digestion.

Flow cytometry and intracellular cytokine staining

Spleen or lymph nodes were subjected to flow cytometry using CytoFlex (Beckman Coulter) and the following fluorescence-labeled antibodies from eBioscience: PB-conjugated anti-CD4; PE-conjugated anti-B220, anti-CD45 and anti-IL-17A; PerCP5.5-conjugated anti-CD8; APC-conjugated anti-CD3 and anti-CD62L; FITC-conjugated anti-CD44, anti-IFNγ and anti-Foxp3; APC-CY7-conjugated anti-CD11b.

For intracellular cytokine staining, T cells were stimulated with PMA (0.5 µg/mL) plus ionomycin (1 µg/mL) for 3 h and monensin (eBioscience, 1000X) for another 3 h, and then subjected to intracellular IFN-γ and IL-17A by flow cytometry analysis.

Amygdala was collected and digested into single cells as “Single cell dissociation” section in the method. Single cells were subjected to flow cytometry and the following fluorescence-labeled antibodies from Abcam: FITC-conjugated anti-AdorA1 (EPR6179); Alexa fluor 647-conjugated anti-myelin oligodendrocyte glycoprotein (MOG, EP4281) and Alexa fluor 568-conjugated anti-NeuN (EPR12763). c-FOS (ab208942), AdorA2A (ab3461), AdorA2B (ab222901) and AdorA3 (ab203298) were purchased from Abcam plc. Some antibodies were purchased from Biolegend: Brilliant violet 421-conjugated anti-GFAP (2E1.E9) and PE-CY7-conjugated anti-CX3CR1 (SA011F11).

Metabolic Assays

Naive CD4⁺ T cells were first purified from the spleens and lymph nodes of 6 to 8-week-old mice by positive magnetic cell sorting. These CD4⁺ T cells were further sorted on a FACS Ariall cell sorter (BD Biosciences) to obtain naive CD4⁺ T cells (CD4⁺CD44^{lo}CD62L^{hi}). The oxygen consumption rate (OCR) and extracellular acidification rate (ECAR) were measured in XFp extracellular flux analyzers (EFA) (Seahorse Bioscience) by using XFp Cell Mito Stress Test Kit and XFp Glycolysis Stress Test kit, respectively. The parameters used in the assays were: 8 × 10⁴ seed cells per well, 1.0 µM oligomycin, 1.0 µM FCCP, 0.5 µM rotenone/antimycin A, 10 mM glucose, and 50 mM 2-DG, as indicated.

Isolation of oligodendrocytes

6 to 8-week-old WT, *Miga2*^{-/-} and *Miga2*^{-/-} plus αCD4 mice were sacrificed using CO₂. The single cell dissociations of two-side amygdala are collected as described in single cell dissociation section. Oligodendrocytes from adult mouse brains were purified by positive magnetic cell sorting (Anti-O4 MicroBeads, # 130-094-543, Miltenyi Biotec). Then, the resuspended cells were incubated with anti-Mouse CD16/CD32 (553141, BD PharMingen), and stained with Alexa Fluor647-conjugated anti-MOG (Ab199472). After washing, incubated cells were further sorted on a FACS Ariall cell sorter (BD Biosciences) to obtain purified MOG⁺ cells. The sorted cells were washed with cold PBS and prepared for the following experiments.

Viral injection

The preparation of craniotomy is referred to the standard stereotaxic coordinates of 7-week-old B6 mice. AAV-MBP-GFP-miR30-shRNA(mAdoral) or AAV-MBP-GFP-miR30-shRNA(control) was constructed by Vigene Bioscience (Shandong, China) and injected into the left amygdala at 1E+11 v.g./mouse within 600 s via a pump. After recovery of the animal, the animal was fed as usual for 2 weeks. The expression of shRNA was measured based on the GFP level by FACS. These AAV-injected mice performed the open field-test two weeks after AAV injection.

LC-MS analysis for serum metabolome

The same amount of supernatant from each treated sample used as a QC sample. The blank sample was a matrix of the experimental sample, and the pretreatment process was the same as the experimental sample. LC separation was conducted on a Accucore HILIC

column with a Vanquish UHPLC system (Thermo). The mobile phase consisted of 0.1% formic acid and 10mM ammonium acetate in 95% acetonitrile (A) and 0.1% formic acid and 10mM ammonium acetate in 50% acetonitrile (B). The gradient program was as follows: 0–1 min, 98% A+2% B; 17–17.5 min, linear gradient to 50%A+50% B; 18–20 min, 98%A+2%B; flow rate, 0.3 mL/min. The column oven temperature was maintained at 40°C. The LC system was coupled with a triple-quadrupole mass spectrometer QE HF-X (Thermo).

¹³C tracing by liquid-chromatography Q-exactive mass spectrometry (LC-QE-MS)

For ¹³C tracing experiments, splenic naive CD4⁺ T cells isolated from WT or *Miga2*^{TKO} mice were cultured with [U6]-¹³C glucose (Sigma-Aldrich) for 24 h. The cells were washed twice in saline and lysed in extraction solvent (80% methanol/water) for 30 min at -80°C. The supernatant extracts were analyzed by LC-QE-MS after centrifugation at 12000 g, 10 min at 4°C. Liquid chromatography was performed using an HPLC (Ultimate 3000 UHPLC) system (Thermo) with an xbridge amide column (100 × 2.1 mm i.d., 3.5 μm; Waters). Mobile phase A was 20 mM ammonium acetate and 15 mM ammonium hydroxide in water with 3% acetonitrile, pH 9.0, and mobile phase B was acetonitrile. The linear gradient was as follows: 0 min, 85% B; 1.5 min, 85% B; 5.5 min, 30% B; 8 min, 30% B, 10 min, 85% B, and 12 min, 85% B. The flow rate was 0.2 mL/min. Sample volumes of 5 μL were injected for LC-MS analysis.

qRT-PCR

For qRT-PCR, total RNA was isolated using TRI reagent (Molecular Research Center, Inc.) and subjected to cDNA synthesis using RNase H-reverse transcriptase (Invitrogen) and oligo (dT) primers. qRT-PCR was performed in triplicates, using iCycler Sequence Detection System (Bio-Rad) and iQTM SYBR Green Supermix (Bio-Rad). The expression of individual genes was calculated by a standard curve method and normalized to the expression of *Actb*. The gene-specific PCR primers (all for mouse genes) are shown in [Table S8](#).

Immunoblot (IB)

Whole-cell lysates or subcellular extracts were prepared as previously described ([Uhlik et al., 1998](#)). The samples were resolved by 8.25% SDS-PAGE. After electrophoresis, separated proteins were transferred onto polyvinylidene difluoride membrane (Millipore). For immunoblotting, the polyvinylidene difluoride membrane was blocked with 5% non-fat milk. After incubation with specific primary antibody, horseradish peroxidase-conjugated secondary antibody was applied. The positive immune reactive signal was detected by ECL (Amersham Biosciences).

Chromatin IP (ChIP) assay

ChIP assays were performed with naive T cells (5 × 10⁶), which were fixed with 1% formaldehyde and sonicated. Lysates were subjected to IP with the IRF-1 antibodies (M-20, Santa Cruz), and the precipitated DNA was then purified by Qiaquick columns (QIAGEN) and quantified by QPCR using pairs of primers that amplify the potential target regions of the *Ada*, *Pnp2* or *Xdh* promoter. The precipitated DNA is presented as percentage of the total input DNA. The gene-specific primers are shown in [Table S8](#).

Tissue staining/IHC

Brain were collected at the indicated time course of each figure legend. After deeply anesthetized, animals were perfused through the heart with 4% paraformaldehyde in PBS. Then brains were removed from the skull, fixed overnight in 4% PFA, and then dehydration in 30% sucrose in PBS solution for 48 h until sunk to the bottom. H&E and Nissl staining of Brain coronal section were performed by Servicebio Biotechnology Co., Ltd (China). For immunohistochemistry, the sections were pre-treated using heat mediated antigen retrieval with sodium citrate buffer and blocked with 5% bovine serum albumin. The sections were stained overnight with antibodies against following: Alexa Fluor 647-conjugated anti-Myelin oligodendrocyte glycoprotein; Alexa Fluor 488-conjugated anti-Adenosine A1 Receptor; Alexa Fluor 568-conjugated anti-NeuN. All antibodies were diluted in TBS contain 0.025% Triton X-100. Samples were further stained with DAPI for 15 min and mounted before image acquisition. Images were captured using the Vectra microscope (PerkinElmer).

***In vivo* BrdU proliferation assay**

8-week-old C57BL/6 mice were injected intraperitoneally with 2mg BrdU (Sangon, E607203) in PBS. After 72 h, mice received an intracardiac perfusion with PBS to remove erythrocytes. The amygdala was collected and dissociated as described in single cell dissociation section. O4⁺ cells were purified with anti-O4 microbeads (Miltenyi, 130-094-543). After that, oligodendrocytes were isolated with Aria II based on the surface marker MOG. For BrdU staining, the purified cells were fixed with 70% ethanol for 30 min, denatured for 30 min with 2M HCl, neutralized for 10 min with 0.1M borate buffer, then washed with PBS three times before anti-BrdU (1:100, BD, 558599) and 7-AAD (1:50, BD, 559925) staining. Samples were acquired using flow cytometer (Beckman CytoFLEX), and the data were analyzed with FlowJo.

QUANTIFICATION AND STATISTICAL ANALYSIS

Statistical analysis was performed using Prism software. For two-group comparison, two-tailed unpaired t tests were performed, and P values less than 0.05 were considered significant. The level of significance was indicated as * $p < 0.05$, ** $p < 0.01$, *** $p < 0.005$.

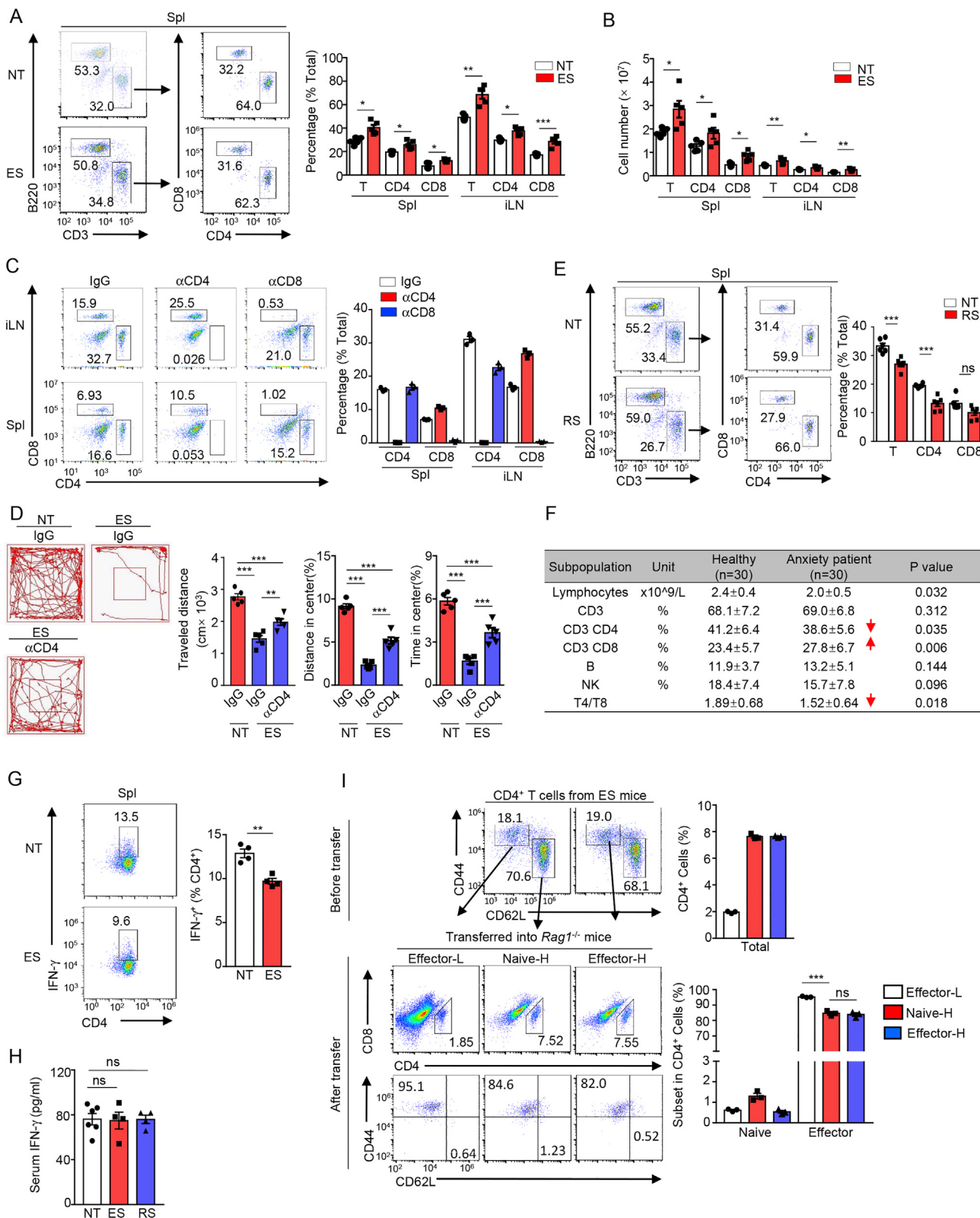
For multiple group comparison, Dunnett's multiple comparison test (one-way ANOVA) was performed, and P values less than 0.05 were considered significant. The Gehan-Breslow-Wilcoxon test was used for the animal survival assay. In the EAE model, the clinical scores were analyzed by Sidak's multiple comparison test (two-way ANOVA) with 90% power and a significance level of 5%. P values less than 0.05 were considered significant, and the level of significance was indicated as * $p < 0.05$, ** $p < 0.01$, *** $p < 0.005$.

All statistical tests are justified as appropriate, and data meet the assumptions of the tests. The groups being statistically compared show similar variance.

DATA AND CODE AVAILABILITY

The accession number for the RNAseq and single cell transcriptome data reported in this paper is [GenBank-Bioproject]: [PRJNA528163].

Supplemental Figures



(legend on next page)

Figure S1. CD4⁺ T Cells are Affected by Stress-Induced Anxiety, Related to Figure 1

(A-B) Flow cytometry analysis of the frequency (A) and absolute numbers (B) of different T cell populations in the spleen (Spl) and inguinal lymph node (iLN) of NT or ES-treated mice ($n = 5$) on day 8. (C) Flow cytometry analysis of the frequency of different immune cells in the Spl and iLN of ES-treated mice, which were pretreated with isotype IgG, anti-CD4 (α CD4) or anti-CD8 (α CD8) as described in major Figures 1A ($n = 3$). (D) WT mice were induced anxiety by chronic ES treatment for continuous 28 days. These mice were administrated with isotype IgG or anti-CD4 (α CD4) (500 μ g/mice) on day 21 and 28. Representative tracks and statistic results in open-field test (OFT) of NT and chronic ES mice on day 30 ($n = 5$). (E) Flow cytometry analysis of the frequency of T cell populations in the Spl of NT or restraint stress (RS)-treated mice on day 8 ($n = 6$). (F) The table showing the frequency of lymphocytes subpopulation in 18–65 years old patient with anxiety and healthy control by FACS analysis ($n = 30$). (G) CD4⁺ T cells were isolated from the spleen of 6-weeks-old NT and ES mice, and incubated with monensin (1 μ g/mL) for 4 h before harvest. Flow cytometric analysis of the percentage of IFN- γ - and IL-17-producing CD4⁺ T cells ($n = 4$). (H) ELISA assay to determine the levels of IFN- γ and IL-17A in serum from NT ($n = 6$), ES ($n = 4$) and RS ($n = 4$) mice on day 8 after inducing anxiety models. (I) *Rag1*^{-/-} mice were adoptively transferred with 1.8×10^6 effector (Effector-L), 6×10^6 naive (Naive-H) and 6×10^6 effector (Effector-H) CD4⁺ T cells isolated from ES-treated mice for every three day. Flow cytometry analysis of the frequency and activated status of CD4⁺ in the spleen of recipient *Rag1*^{-/-} mice on day 8 ($n = 3$). All data are representative of at least three independent experiments. Data are represented as means \pm SEM. The significance of difference in (H) was determined by Dunnett's multiple comparisons test. The significances of differences in all two group comparisons were determined by two-tailed Student's t test. * $p < 0.05$; ** $p < 0.01$; *** $p < 0.005$.

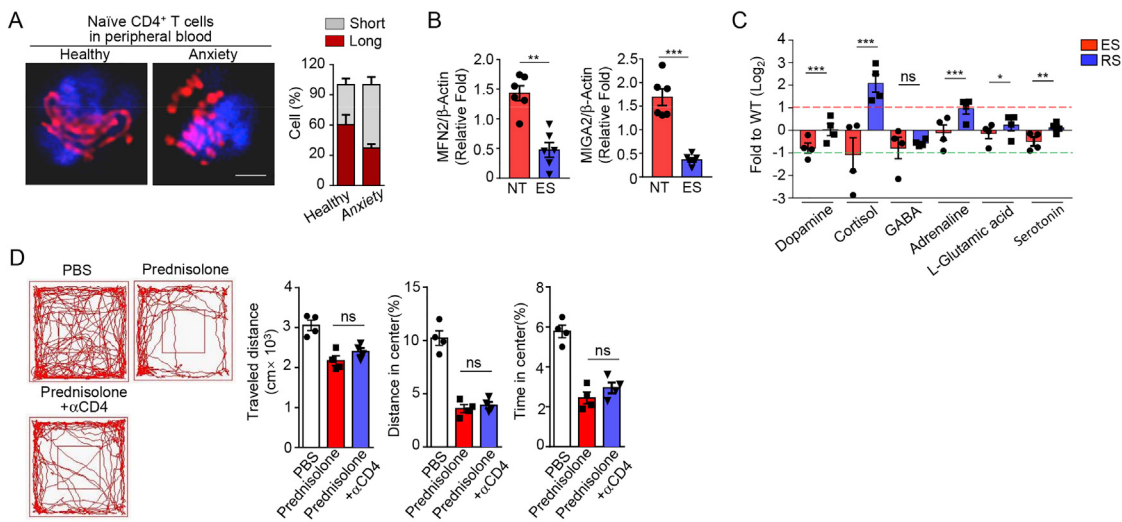
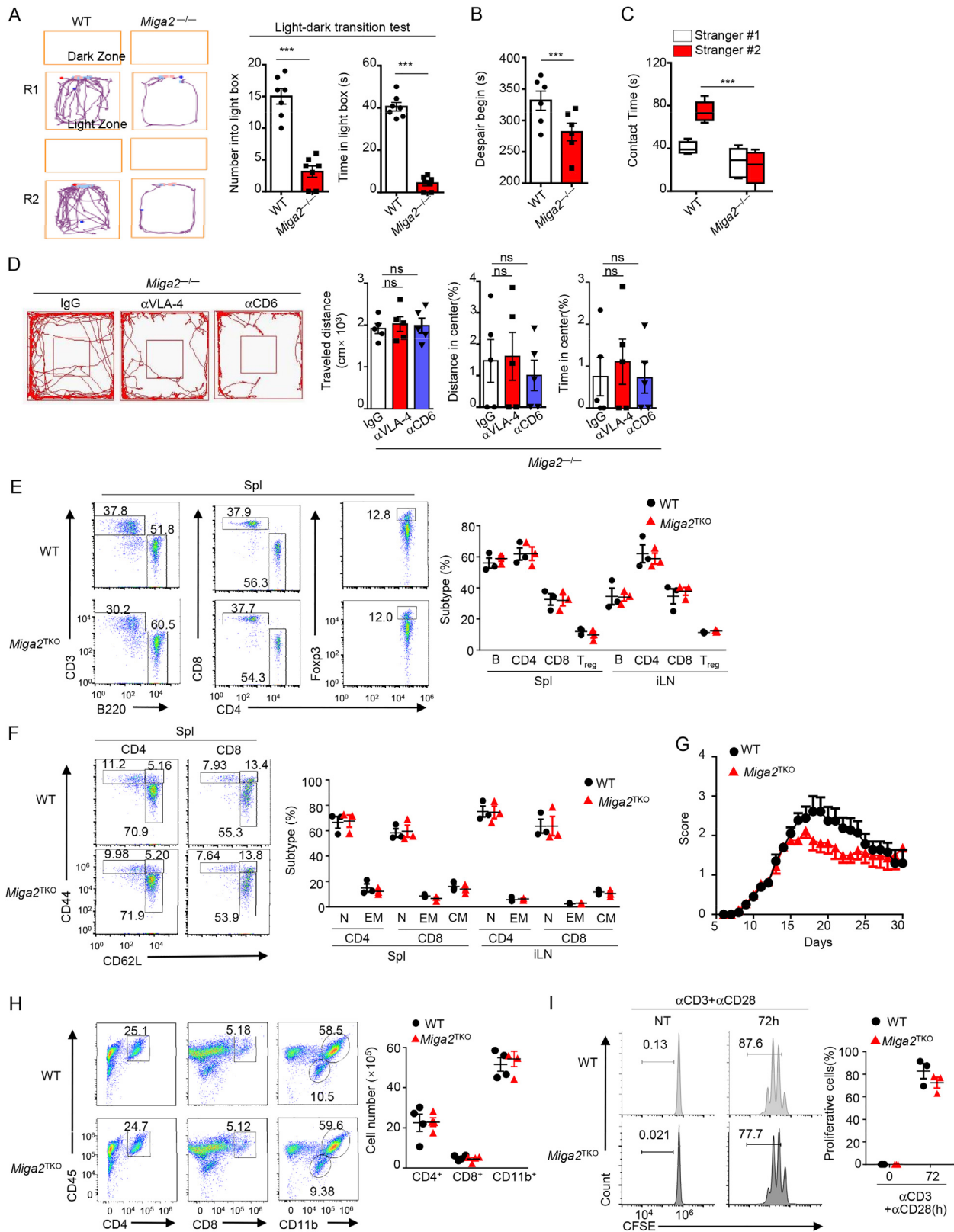


Figure S2. Mitochondrial Fission in CD4⁺ T Cells is Associated with the Anxiety Symptom, Related to Figure 2

(A) Naive CD4⁺ T cells (CD4⁺CD44^{lo}) in peripheral blood from patients with anxiety and healthy control were isolated by FACS sorter (n = 4). Mitochondrial morphology of these naive CD4⁺ T cells was visualized using MitospoTM Orange CMTMRos staining. Representative confocal images are shown, as well as length quantification with Image-Pro. Data are shown as the mean ± SEM of three independent experiments with 50 cells counted for each replicate; Colors indicate the morphology of the mitochondria (long, brown > 7 μm or short, gray < 7 μm). Bar, 5 μm . (B) Immuno-blots (IB) analyses of MIGA2 and MFN2 in the splenic naive CD4⁺ T cells from three individual NT or ES-treated mice. #1, repeat 1; #2, repeat 2; #3, repeat 3. The relative density of these IB assay were evaluated by ImageJ. (C) LC-MS of indicated neurotransmitters and hormones in the serum of NT, ES-treated and RS treated mice, presented relative to the mean value for NT mice (n = 4). (D) WT mice were i.p. injected with prednisolone (50 mg/kg) every other day within 21 days. Anxiety-like behavior of these mice was assessed as traveled distance, percentage of distance and percentage of time spent in center area in OFT on day 22 (n = 4). All data are representative of at least three independent experiments. Data are represented as means ± SEM. The significances of differences were determined by two-tailed Student's t test. *p < 0.05; **p < 0.01; ***p < 0.005.



(legend on next page)

Figure S3. *Miga2*^{-/-} Mice Performed Various Psychological Disorders, but Not CNS Inflammation, Related to Figure 3

(A) Representative tracks of 8-weeks-old WT and *Miga2*^{-/-} mice in the light compartment, as well as transition numbers and the time spent in the light compartment (n = 7). (B) The time of immobility in the tail suspension test was record for WT and *Miga2*^{-/-} mice (n = 6). (C) In the social novelty task, the contact time with Stranger 1 and Stranger 2 chambers of the WT and *Miga2*^{-/-} mice are shown. (D) *Miga2*^{-/-} mice were i.v. injected with anti-VLA-4 (α VLA-4, 20mg/kg) or anti-CD6 (α CD6, 10mg/kg) for every three days, and then evaluated anxiety-like behavior by open-field test on day 8 (n = 5). (E) Flow cytometry analysis of the frequencies of different lymphocytes in the spl of 6-8 weeks-old WT or *Miga2*^{TKO} mice (n = 3). Data all panels are presented as representative FACS plots. B cell is defined as CD3⁻B220⁺; CD4 T cell (CD4) is defined as CD3⁺B220⁺CD4⁺; CD8 T cell (CD8) is defined as CD3⁺B220⁺CD8⁺; regulatory T cell (Treg) is defined as CD3⁺B220⁺CD4⁺Foxp3⁺. (F) Flow cytometry analysis of naive and memory T cells in the Spl of WT or *Miga2*^{TKO} mice (n = 3). Naive T cell (N) is defined as CD44^{lo}CD62L^{hi}; Effector memory (EM) T cell is defined as CD44^{hi}CD62L^{lo}; Effector memory (EM) T cell is defined as CD44^{hi}CD62L^{lo}; Central memory (CM) T cell is defined as CD44^{hi}CD62L^{hi}. (A) Mean clinical scores of 6-8 weeks-old WT and *Miga2*^{TKO} mice subjected to MOG₃₅₋₅₅-induced experimental autoimmune encephalomyelitis (EAE) (n = 10/group). (H) Flow cytometry analysis of the immune cell infiltration into the CNS (brain and spinal cord) of EAE mice (n = 4, day 14 post-immunization). (I) Naive CD4⁺ T cells (CD44^{lo}CD62L^{hi}) were isolated from the spleen of WT and *Miga2*^{TKO} mice by FACS sorter. These T cells were labeled with 5 μ M Carboxyfluorescein succinimidyl ester (CFSE), and stimulated with α CD3 (1 μ g/mL)/ α CD28 (1 μ g/mL) for 72 h. The proliferative ratio was assessed as CFSE dilution by FACS. All data are representative of at least three independent experiments. Data are represented as means \pm SEM. The significances of differences in comparisons were determined by two-tailed Student's t test. ns, no significance; ***p < 0.005.

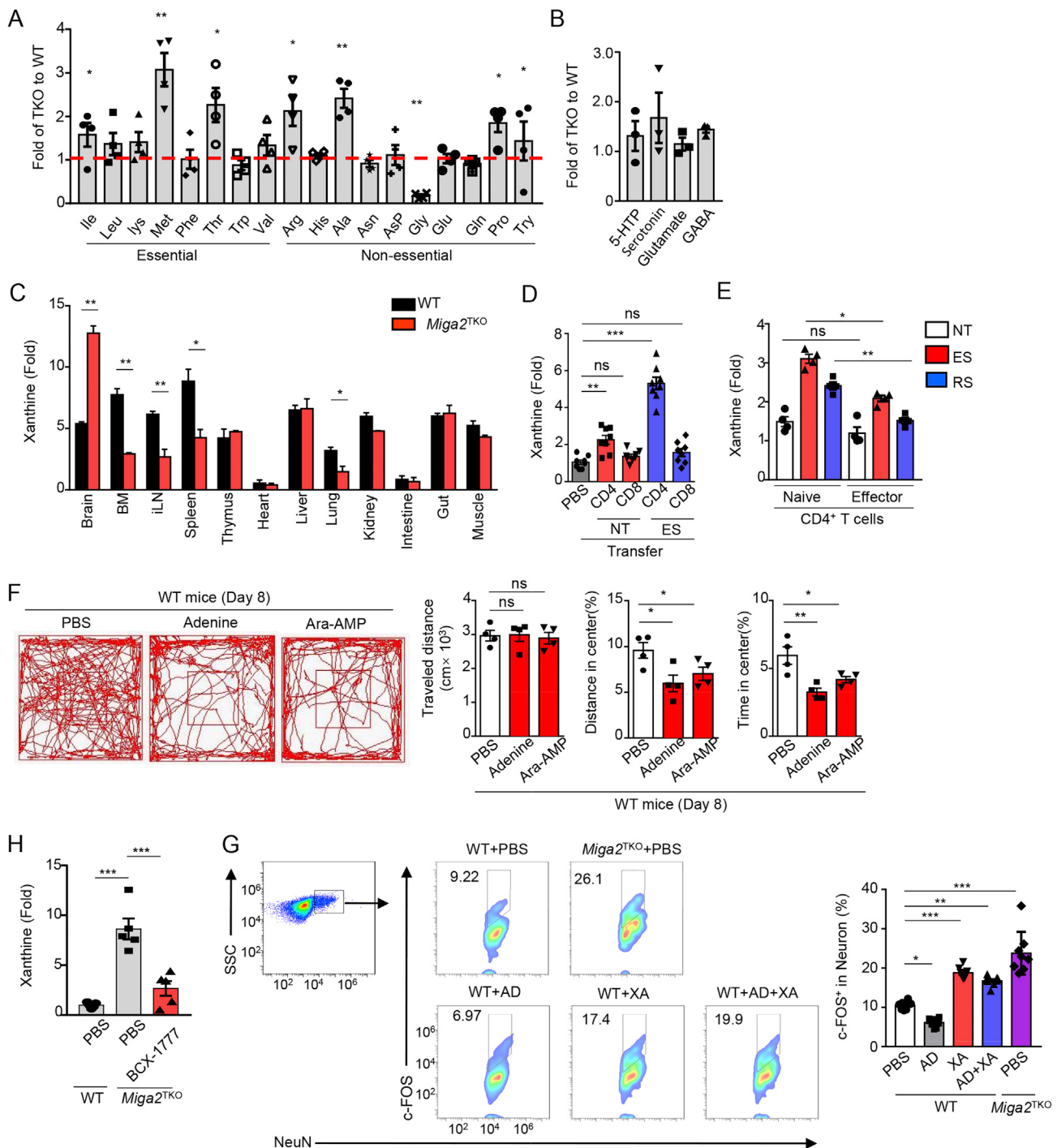
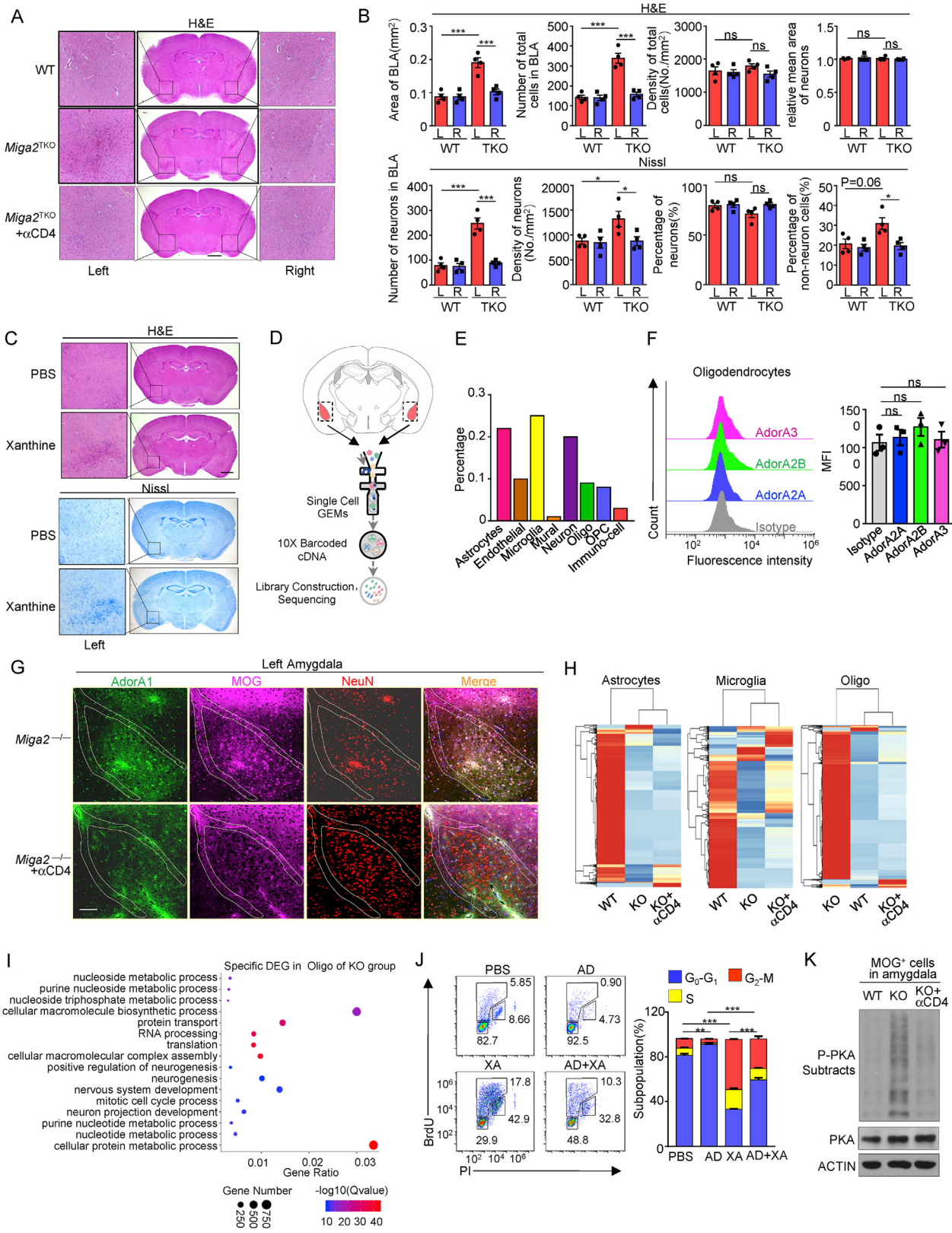


Figure S4. CNS-Enriched Xanthine Causes Anxiety-like Behavior Abnormality, Related to Figure 4

(A-B) The essential and non-essential amino acids (A) or the neurotransmitters derived from amino acids (B) in the serum were measured by PLS-DA and presented as the ratio of the abundance in *Miga2^{TKO}* mice to those in WT mice ($n = 4$). (C) ELISA assay of xanthine in the different organs of WT and *Miga2^{TKO}* mice are presented as relative fold to those in the heart of *Miga2^{TKO}* mice ($n = 4$). (D) *Rag1^{-/-}* mice were i.v. adoptively transferred with 5×10^6 CD4⁺ or CD8⁺ T cells isolated from NT or ES-treated mice (donor) for every three days. Xanthine in the serum of recipient mice was measured by ELISA. The relative fold is to serum xanthine concentration of *Rag1^{-/-}* control that treated with PBS. (E) 4×10^6 purified effector or naive CD4⁺ T cells were isolated from ES or RS-treated mice as previous described. These CD4⁺ T cells were cultured in 500 μ L medium *in vitro*, and the supernatants were collected after 24 h. Xanthine was measured by ELISA and presented as relative folds to that of effector group from NT mice. (F) WT mice were i.p. injected with Adenine and its derivatives (500 mg/kg) for three times in every three days. Anxiety-like behavior of these mice was assessed as traveled distance, percentage of distance and percentage of time spent in center area in

(legend continued on next page)

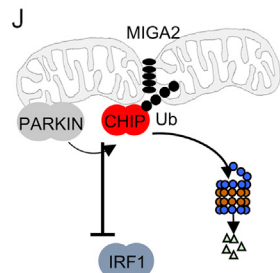
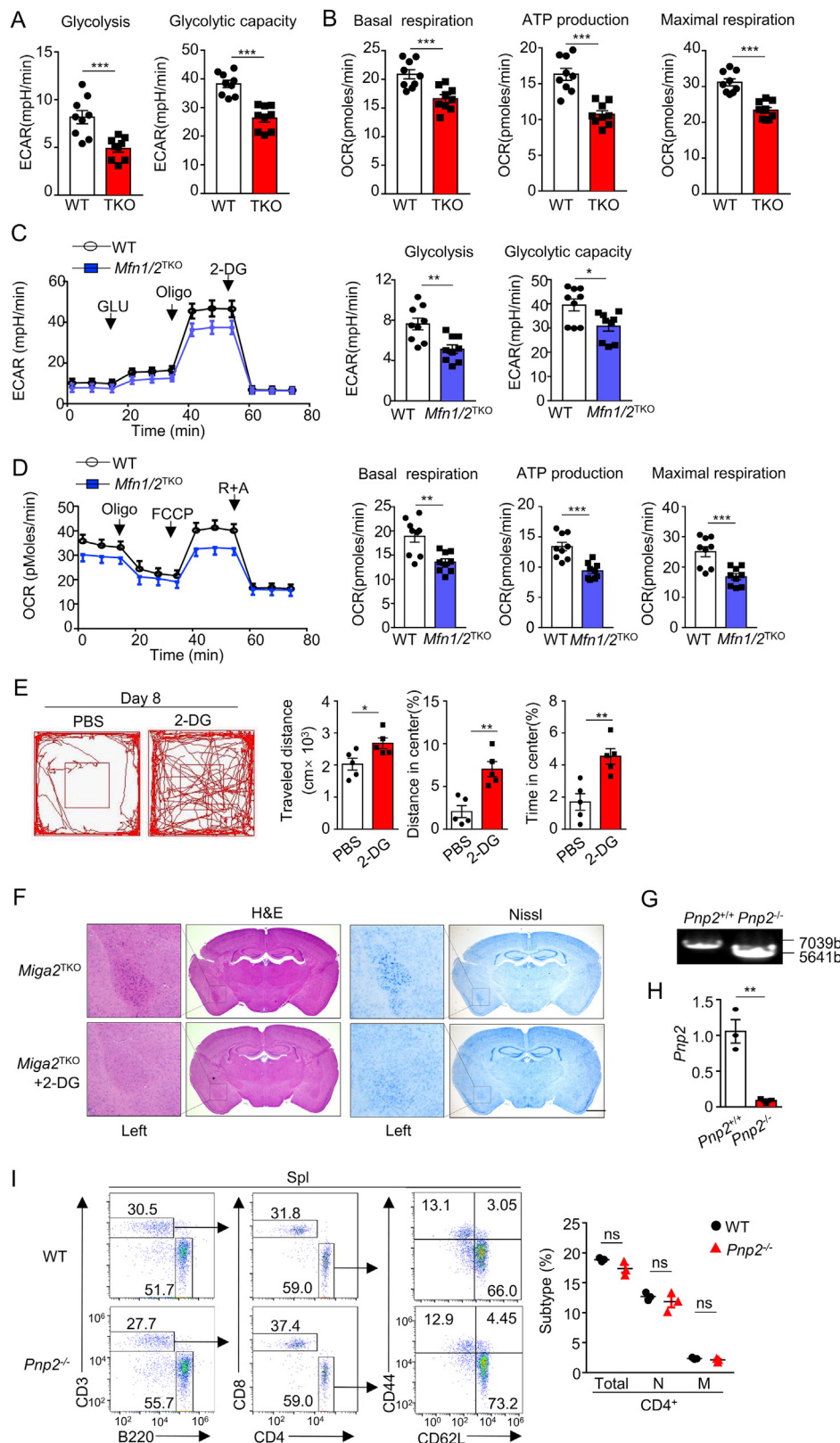
OFT on day 8 (n = 4). (G) WT mice were injected i.p. with adenine (AD) or xanthine (XA) as indicated. *Miga2*^{TKO} mice were injected i.p. with PBS alone. Flow cytometry analysis of c-FOS⁺ cells gating with NeuN⁺ cells in the amygdala (n = 7). (H) *Miga2*^{TKO} mice were i.p. injected with BCX-1777 as described in major Figure 4I. The abundance of xanthine in serum of BCX-1777-treated *Miga2*^{TKO} mice was measured by ELISA and presented as the relative fold to that in PBS-treated group. All data are representative of at least three independent experiments. Data are represented as means ± SEM. The significance of difference in D–G was determined by Dunnett's multiple comparisons test. The significances of differences in all other two group comparisons were determined by two-tailed Student's t test. *p < 0.05; **p < 0.01; ***p < 0.005.



(legend continued on next page)

Figure S5. The Absence of *Miga2* or Xanthine Causes Pathological Symptoms by Directly Acting on Oligodendrocytes the Left Amygdala, Related to Figure 5

(A) Histological analysis of the whole brain from WT, *Miga2*^{2TKO} and CD4⁺ T cell-depleting *Miga2*^{2TKO} mice was performed by H&E staining. Scale bar, 100 μm. (B) The statistical results of histological analysis in Figure 5A and Figure S7A were analyzed by Tissue FAXS System (TissueGnostics, AT), and presented as indication (n = 4). (C) Histological analysis of the amygdala was performed by H&E and nissl staining, when WT mice were injected with synthetic xanthine as described in Figure 4H. Scale bar, 100 μm. (D) Schematic showing the single-cell RNA sequencing (scRNA-seq) workflow. (E) The percentage of nine major clusters of cell types in the amygdala of WT mice revealed by scRNA-seq. (F) Flow cytometry analyses of AdorA2A⁺, AdorA2B⁺ and AdorA3⁺ cells gating with MOG⁺ cells in the amygdala of WT mice (n = 3). Oligodendrocytes (Oligo) are defined as MOG⁺. (G) Representative image of FITC-AdorA1 (Green), APC-MOG (Purple), PE-NeuN (Red) and DAPI (Blue) staining in mouse amygdala sections from *Miga2*^{-/-} and α CD4-treated *Miga2*^{-/-} mice. The scale bar is 5 μm. (H) The transcriptomes of astrocytes, microglia or oligodendrocytes in the amygdala were clustered among the WT, *Miga2*^{-/-} (KO) and KO plus α CD4 groups. Heatmap showing the DEGs determined by scRNA-seq data. (I) The specific DEGs in oligodendrocytes of KO group were collected compared to those of WT and KO treated with α CD4 groups. KEGG analysis of these DEGs in indicated pathway that differ significantly (in abundance). (J) WT mice were injected intravenously injection of 2 mg BrdU together with AD or XA as indicated. 72 h later, purified oligodendrocytes were stained with anti-BrdU antibody and propidium iodide (PI). (K) Myelin oligodendrocyte glycoprotein (MOG) positive cells were isolated from the amygdala of 6-8 weeks WT, KO and KO treated with α CD4 mice by FACS sorter. PKA activity was monitored via the level of p-PKA subtracts by IB assay. Except panel D, other data are representative of at least three independent experiments. Data are represented as means ± SEM. The significances of differences were determined by Dunnett's multiple comparisons test. ns, no significance; *p < 0.05; **p < 0.01; ***p < 0.005.



(legend on next page)

Figure S6. Mitochondrial Fission in CD4⁺ T Cells Promotes Purine Synthesis, Related to Figure 6

(A-B) Mitochondrial fitness tests were used to compare ECAR (**A**) and OCR (**B**) of WT and *Miga2*^{TKO} (TKO) CD4⁺ T cells (n = 9). The statistic results of major figure 6a were presented as bar graph. **(C-D)** Mitochondrial fitness tests were measured by ECAR (**C**) and OCR (**D**) of CD4⁺ T cells isolated from WT and *Mfn1/2*^{TKO} mice (n = 9). The statistic results were presented as bar graph. **(E)** *Miga2*^{TKO} mice were i.p. injected with 2-Deoxy-D-glucose (2-DG) (500 mg/kg) for three times in every three days. Anxiety-like behavior of these mice was assessed as traveled distance, percentage of distance and percentage of time spent in center area in open-field test on day 8 (n = 5). **(F)** Histological analysis of the whole brain section from *Miga2*^{TKO} and 2-DG-treated *Miga2*^{TKO} mice described as above was performed by H&E and Nissl staining. Scale bar, 100 μ m. **(G)** *Pnp2*^{-/-} genotyping PCR. PCR was performed to detect the WT and *Pnp2* depletion alleles (with primers described in Table S7). **(H)** QPCR assay showing ablation of *Pnp2* in the CD4⁺ T cells of *Pnp2*^{-/-} mice. These qPCR data were presented as fold relative to the *Actb* mRNA level and normalized by Bio-Rad CFX Manager 3.1. **(I)** Flow cytometry analysis of the frequencies of different lymphocytes in the spl of 6-8 weeks-old WT or *Pnp2*^{-/-} mice (n = 3). All panels are presented as representative FACS plots. The statics analysis was performed as plot graph. **(J)** A signal transduction model of mitochondrial fission in promoting IRF-1 stability. All data are representative of at least three independent experiments. Data are represented as means \pm SEM. The significances of differences in two group comparisons were determined by two-tailed Student's t test. *p < 0.05; **p < 0.01; ***p < 0.005.